Cell Reports

Article

TFEB Transcriptional Responses Reveal Negative Feedback by BHLHE40 and BHLHE41

Graphical Abstract

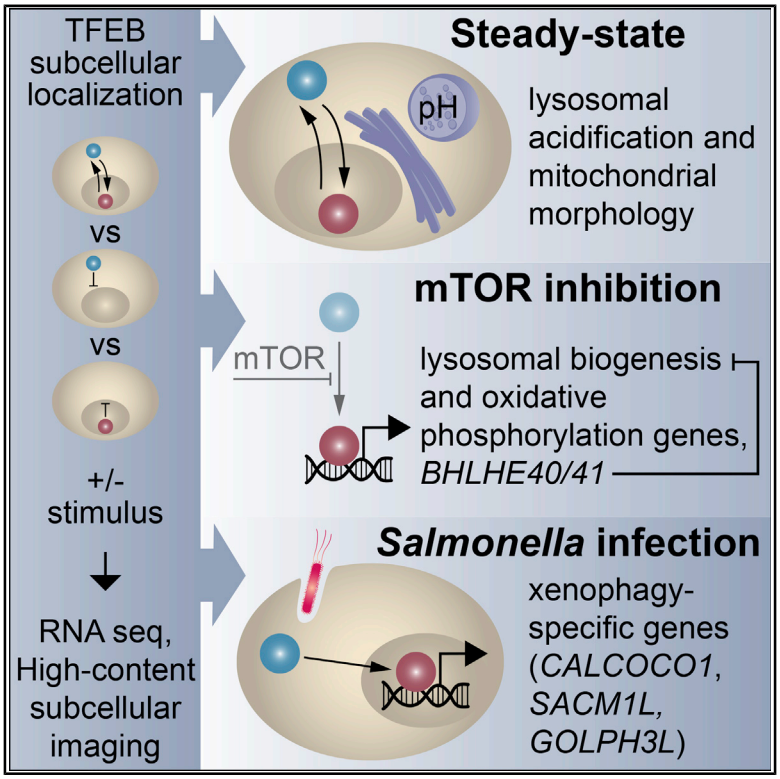

Highlights

- TFEB transcriptional programs are defined by subcellular localization and stimulation
- Nuclear TFEB maintains lysosomal and mitochondrial compartments at steady state
- BHLHE40 and BHLHE41 counter-regulate stimulation-specific TFEB target genes

Authors

Kimberly L. Carey, Geraldine L.C. Paulus, Lingfei Wang, ..., Kara G. Lassen, Herbert W. Virgin, Ramnik J. Xavier

Correspondence

xavier@molbio.mgh.harvard.edu

In Brief

Employing RNA sequencing, genome-wide CRISPR screening, and high-content subcellular imaging, Carey et al. systematically unravel localization- and stimulation-specific transcriptional responses to TFEB, including target gene activation at steady state. The authors further uncover a negative feedback loop by BHLHE40 and BHLHE41 that counteracts a TFEB transcriptional signature induced by lysosomal stress.

Carey et al., 2020, Cell Reports *33*, 108371
November 10, 2020
https://doi.org/10.1016/j.celrep.2020.108371

CellPress

Cell Reports

CellPress
OPEN ACCESS

Article

TFEB Transcriptional Responses Reveal Negative Feedback by BHLHE40 and BHLHE41

Kimberly L. Carey,[1,2,11] Geraldine L.C. Paulus,[3,4,11] Lingfei Wang,[1,2] Dale R. Balce,[5,10] Jessica W. Luo,[1,2] Phil Bergman,[6] Ianina C. Ferder,[3,4] Lingjia Kong,[3,4] Nicole Renaud,[6] Shantanu Singh,[7] Maria Kost-Alimova,[8] Beat Nyfeler,[9] Kara G. Lassen,[1,2,3,4] Herbert W. Virgin,[5,10] and Ramnik J. Xavier[1,2,3,4,12,*]

[1]Immunology Program, Broad Institute of MIT and Harvard, Cambridge, MA 02142, USA
[2]Infectious Disease and Microbiome Program, Broad Institute of MIT and Harvard, Cambridge, MA 02142, USA
[3]Department of Molecular Biology, Massachusetts General Hospital, Harvard Medical School, Boston, MA 02114, USA
[4]Center for Computational and Integrative Biology, Massachusetts General Hospital, Harvard Medical School, Boston, MA 02114, USA
[5]Department of Pathology and Immunology, Washington University School of Medicine, St. Louis, MO 63110, USA
[6]Novartis Institutes for BioMedical Research, Cambridge, MA 02139, USA
[7]Imaging Platform, Broad Institute of MIT and Harvard, Cambridge, MA 02142, USA
[8]Center for the Science of Therapeutics, Broad Institute of MIT and Harvard, Cambridge, MA 02142, USA
[9]Novartis Institutes for BioMedical Research, Basel, Switzerland
[10]Present address: Vir Biotechnology, San Francisco, CA 94158, USA
[11]These authors contributed equally
[12]Lead Contact
*Correspondence: xavier@molbio.mgh.harvard.edu
https://doi.org/10.1016/j.celrep.2020.108371

SUMMARY

Transcription factor EB (TFEB) activates lysosomal biogenesis genes in response to environmental cues. Given implications of impaired TFEB signaling and lysosomal dysfunction in metabolic, neurological, and infectious diseases, we aim to systematically identify TFEB-directed circuits by examining transcriptional responses to TFEB subcellular localization and stimulation. We reveal that steady-state nuclear TFEB is sufficient to activate transcription of lysosomal, autophagy, and innate immunity genes, whereas other targets require higher thresholds of stimulation. Furthermore, we identify shared and distinct transcriptional signatures between mTOR inhibition and bacterial autophagy. Using a genome-wide CRISPR library, we find TFEB targets that protect cells from or sensitize cells to lysosomal cell death. *BHLHE40* and *BHLHE41*, genes responsive to high, sustained levels of nuclear TFEB, act in opposition to TFEB upon lysosomal cell death induction. Further investigation identifies genes counter-regulated by TFEB and BHLHE40/41, adding this negative feedback to the current understanding of TFEB regulatory mechanisms.

INTRODUCTION

Lysosomes facilitate recycling of unwanted cytosolic components, including damaged organelles, oxidized lipid aggregates, or pathogens targeted by autophagy (Kuo et al., 2018; Najibi et al., 2016; Visvikis et al., 2014). Digested lysosomal products released by autophagolysosomes satisfy nutritional and energy needs of the cell (Rabinowitz and White, 2010; Singh and Cuervo, 2011). Transcription factor EB (TFEB), a member of the MiT/TFE family of transcription factors expressed widely across cell types, is a master regulator of lysosomal biogenesis, autophagy, and lipid metabolism (Martina et al., 2014; Rusmini et al., 2019; Sardiello et al., 2009; Settembre et al., 2011, 2013; Tan et al., 2019). We previously demonstrated a role for TFEB in maintaining intestinal epithelial-cell-specific functions. Compared with wild type (WT), mice lacking TFEB in the intestinal epithelium were more susceptible to epithelial injury and had reduced expression of antimicrobial peptides required for host defense (Murano et al., 2017). *In vivo* studies also elucidated functions for TFEB in spatiotemporal control of myelination during central nervous system development and following injury (Goodman et al., 2018; Meireles et al., 2018). Collectively, TFEB activates transcription in response to many physiological signals to maintain cellular homeostasis.

TFEB activity is controlled by its subcellular localization, which is regulated by post-translational modifications, including phosphorylation (Martina et al., 2012; Martina and Puertollano, 2018; Napolitano et al., 2018; Puertollano et al., 2018; Roczniak-Ferguson et al., 2012; Settembre et al., 2011, 2012). In nutrient-rich conditions, mTOR phosphorylates TFEB at S142 and S211, promoting the interaction between TFEB and 14-3-3 proteins that shield its nuclear localization signal (NLS) (Martina et al., 2012; Napolitano et al., 2018; Puertollano et al., 2018; Roczniak-Ferguson et al., 2012; Settembre et al., 2012; Xu et al., 2019). Upon cellular stress signals, such as nutrient deprivation, inhibition of the amino acid sensing mTOR complex 1 (mTORC1) results in accumulation of TFEB dephosphorylated at S142 and S211, which dissociates from 14-3-3 proteins, translocates into the nucleus, and activates

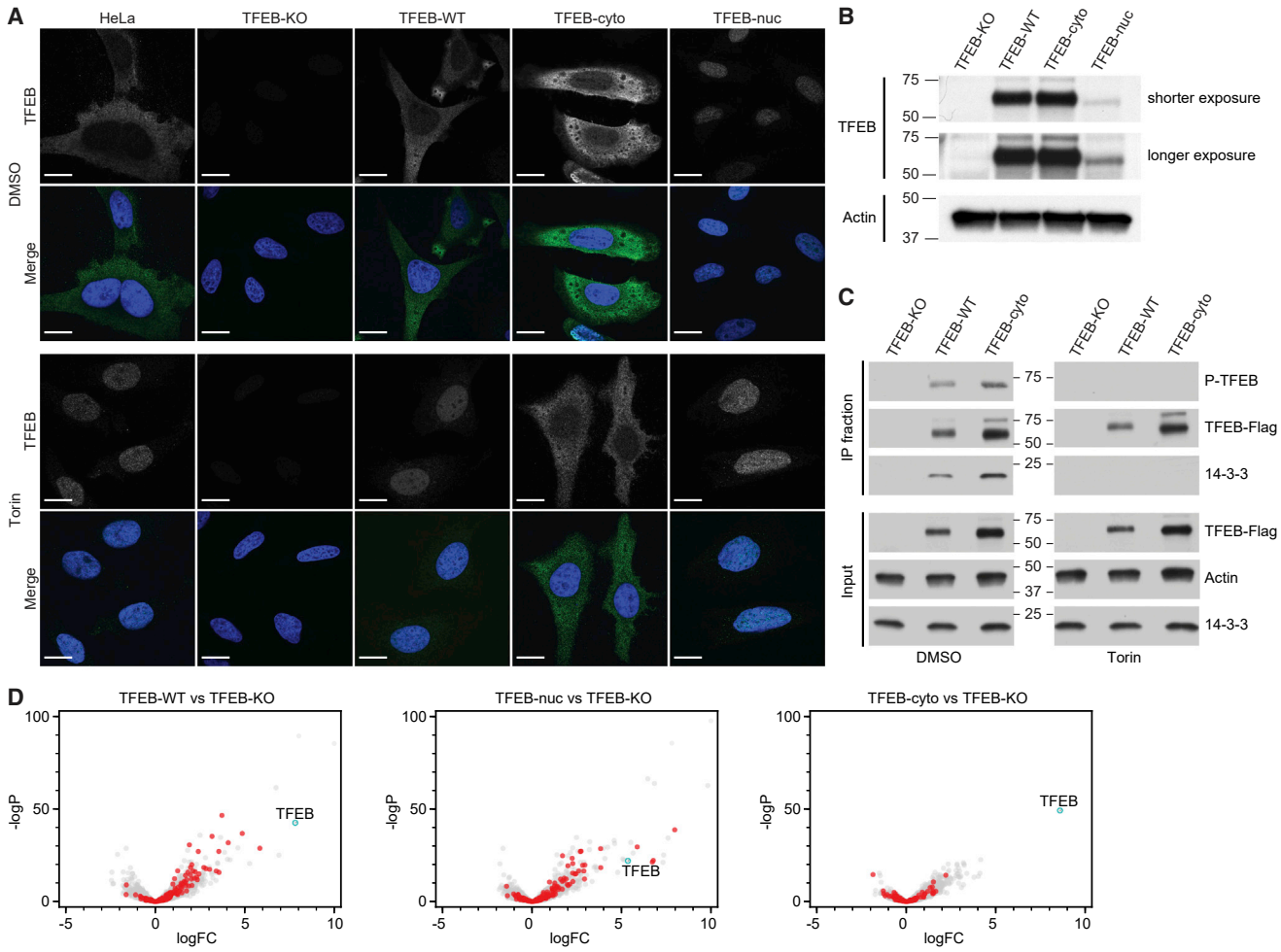

Figure 1. Engineered Cell Lines Demonstrate Transcriptional Response to TFEB Localization

(A) Subcellular localization of TFEB in HeLa and TFEB-knockout HeLa cells reconstituted with empty vector (TFEB-KO), WT TFEB (TFEB-WT), cytosol-restricted TFEB (TFEB-cyto), or nuclear-restricted TFEB (TFEB-nuc) following treatment with DMSO or Torin. Representative confocal microscopy images show TFEB detected with anti-TFEB antibody (green in merged channels; white in single channels) and DNA with Hoechst (blue). Scale bars represent 5 μm.

(B) Representative anti-TFEB immunoblot demonstrates TFEB protein is not detected in TFEB-KO cells. TFEB-WT and TFEB-cyto are expressed at similar levels, whereas detectable TFEB-nuc expression is lower. Actin acts as a loading control.

(C) TFEB-cyto maintains functional interactions in the cytosol. Immunoprecipitation of recombinant Strep/FLAG-tagged TFEB from HeLa cells expressing TFEB-KO, TFEB-WT, or TFEB-cyto following DMSO or Torin treatment. Both TFEB-WT and TFEB-cyto are phosphorylated (P-TFEB) and interact with 14-3-3 proteins before Torin treatment. Upon Torin treatment, TFEB-WT and TFEB-cyto are not detected with the phosphoantibody and do not interact with 14-3-3 proteins. Actin acts as a loading control.

(D) Cells were processed for RNA sequencing. The TFEB transcript level (cyan) is significantly increased in TFEB-WT, TFEB-nuc, and TFEB-cyto cells relative to TFEB-KO cells. Shown in red is a subset of known TFEB target genes (Table S1: Sardiello et al., 2009), many of which have an increased log fold change (logFC) in TFEB-WT and TFEB-nuc relative to TFEB-KO cells. Most genes in TFEB-cyto cells are not significantly upregulated relative to TFEB-KO cells. See also Figure S1.

its transcriptional program (Martina et al., 2012; Roczniak-Ferguson et al., 2012; Xu et al., 2019). The TFEB dephosphorylated state is also achieved through inhibition of mTOR activity by small molecules such as Torin (Martina and Puertollano, 2018; Napolitano et al., 2018). Studies have further described regulation of TFEB activity in response to glucose deprivation and bacterial pathogens through AMP-activated protein kinase (AMPK) (Eichner et al., 2019; El-Houjeiri et al., 2019; Visvikis et al., 2014).

Additional regulation of TFEB activity occurs through nuclear export. Reports have identified an evolutionarily conserved nuclear export signal and demonstrated that TFEB continuously shuttles between the cytosol and the nucleus at steady state (Li et al., 2018; Napolitano et al., 2018; Silvestrini et al., 2018). Treatment with Torin blocked this shuttling event, indicating that movement of TFEB both in and out of the nucleus may be modulated by nutrient availability in an mTOR-dependent manner (Li et al., 2018; Napolitano et al., 2018). How different stimuli regulate TFEB-dependent gene signatures and what mechanisms govern the magnitude and duration of the transcriptional response remain unknown.

The cellular processes governed by TFEB are complex and require coordinated protein expression; thus, a systematic

understanding of how TFEB and its targets are regulated at steady state and in response to stimuli is necessary. In this study, we employed RNA sequencing and a genome-wide CRISPR screen to study TFEB-dependent target genes in response to genetic manipulations and exogenous stimuli. We discovered that a subset of TFEB target genes is activated at steady state, whereas others are stimulation dependent. Further investigation into how TFEB targets affect cellular survival in response to lysosomal stress revealed that BHLHE40 and BHLHE41 counteracted the TFEB response. Here, we demonstrate that these two genes are upregulated in response to stimulus-dependent TFEB activation as part of a negative feedback loop that counter-regulates select TFEB targets involved in lysosomal function.

RESULTS

Engineered Cell Lines Demonstrate Transcriptional Response to TFEB Localization

To study transcriptional responses to TFEB maintained in the nucleus or cytosol, we generated a clonal TFEB-knockout (KO) HeLa cell line using the CRISPR-Cas9 system. TFEB deletion was confirmed by confocal microscopy and immunoblot (Figures 1A and 1B). TFEB was re-expressed in the KO cell line by reconstitution with one of the following constructs: WT TFEB (TFEB-WT); cytosol-restricted TFEB (TFEB-cyto), generated by replacing basic residues in the NLS with alanines (Roczniak-Ferguson et al., 2012); nuclear-restricted TFEB (TFEB-nuc), generated by removing the first 30 amino acids of the N- terminus, which reduces lysosomal targeting and increases nuclear localization in the absence of a stimuli (Roczniak-Ferguson et al., 2012); or a vector control (TFEB-KO). Confocal microscopy established that TFEB-WT and TFEB-cyto constructs were expressed at comparable levels to endogenous TFEB in WT HeLa cells and confirmed expected subcellular localization of TFEB-cyto and TFEB-nuc constructs at steady state (Figure 1A). Upon treatment with Torin, TFEB translocated into the nucleus in TFEB-WT cells, as in WT HeLa cells, whereas TFEB-cyto and TFEB-nuc cells remained in the cytosol and nucleus, respectively (Figure 1A).

Next, we examined TFEB-cyto phosphorylation and interactions with 14-3-3 proteins to verify that mutagenesis of the NLS did not affect other functional domains. Immunoprecipitations of TFEB-WT and TFEB-cyto constructs at steady state confirmed TFEB phosphorylation and interactions with 14-3-3 proteins, whereas neither TFEB nor 14-3-3 protein interactions were detected in the TFEB-KO immunoprecipitated fraction (Figure 1C). Furthermore, the TFEB-cyto construct was no longer detected in the phosphorylated state or interacting with 14-3-3 proteins upon Torin treatment. These data demonstrate that the TFEB-cyto construct maintains functional protein-protein interactions.

To investigate cellular processes that require TFEB nuclear translocation and transcriptional activation, we evaluated LC3 processing as a measure of autophagy initiation. By immunoblot, the ratio of membrane-bound LC3-II to cytosolic LC3-I, which corresponds to autophagosome formation, was similar in TFEB-KO and reconstituted cell lines at steady state, whereas TFEB-WT and TFEB-nuc cells responded to Torin or a combination of Torin and autolysosomal inhibitors E64d/Pepstatin A more robustly than TFEB-KO or TFEB-cyto cells, indicating the reconstituted cell lines behave as expected in a cellular process (Figures S1A and S1B; Settembre et al., 2011).

Previous reports using microarray and chromatin immunoprecipitation sequencing (ChIP-seq) analyses demonstrated that overexpressing epitope-tagged TFEB, in addition to endogenous TFEB, in WT HeLa cells activated target gene transcription (Palmieri et al., 2011; Sardiello et al., 2009; Settembre et al., 2011). Although these identified TFEB-responsive genes, it remains unclear which are controlled by TFEB in the absence of cellular stimulation or stress. We used RNA sequencing to evaluate transcriptional effects of TFEB expression and localization in reconstituted KO cells. Increases in the log fold change (logFC) of the TFEB transcript detected in TFEB-WT, TFEB-nuc, and TFEB-cyto cells relative to TFEB-KO cells served as an internal RNA sequencing control for each cell line (Figure 1D). No steady-state transcriptional changes were detected in other MiT/TFE family members, suggesting there was no compensation in the reconstituted cells. Differential gene expression data demonstrated a robust TFEB-dependent induction of genes, including known targets (Table S1; Sardiello et al., 2009) in TFEB-WT and TFEB-nuc cells and a negligible transcriptional response in TFEB-cyto cells (Figure 1D). Relative to TFEB-WT cells, no significant transcriptional responses were observed in TFEB-nuc cells at steady state, whereas TFEB-cyto cells failed to activate gene transcription (Figure S1C).

TFEB at Steady State Induces a Transcriptional Response that Is Amplified by Sustained Nuclear Localization

To directly compare transcriptional responses between reconstituted cell lines, we calculated the relative expression for all differentially expressed genes at steady state (Figure 2; STAR Methods). The overall transcriptional response of TFEB-nuc cells closely resembled that of TFEB-WT cells, whereas the response of TFEB-cyto cells clustered more closely with TFEB-KO cells (Figure 2A). The absence of a global transcriptional upregulation in TFEB-cyto cells is consistent with the requirement of nuclear localization for TFEB activity. Our data also revealed a subset of genes upregulated in TFEB-cyto relative to TFEB-KO cells, suggesting activation through an indirect mechanism (Figure 2). Importantly, the transcriptional response observed in TFEB-WT relative to TFEB-KO cells indicates the steady-state level of nuclear-localized TFEB is sufficient to induce transcriptional upregulation of TFEB-dependent genes (Figures 1D and 2).

Among the differentially expressed genes, we detected upregulation of known targets in TFEB-WT and TFEB-nuc cells (Figure 2B; Tables S1 and S2), including genes functioning in lysosomal and autophagy pathways, such as lysosomal enzymes *CTSA*, *CTSB*, *CTSD*, *CTSS*, and *NEU1*; *WIPI1*, a regulator of autophagosome formation; and *OPTN*, an autophagy adaptor protein (Sardiello et al., 2009). Genes required for cellular metabolism and homeostasis were also selectively upregulated in TFEB-WT and TFEB-nuc cells, such as *G0S2*, a key regulator of lipid metabolism; *IFI30*, an interferon γ-inducible thiol reductase involved in antigen presentation; and *FOLR1*, a folate

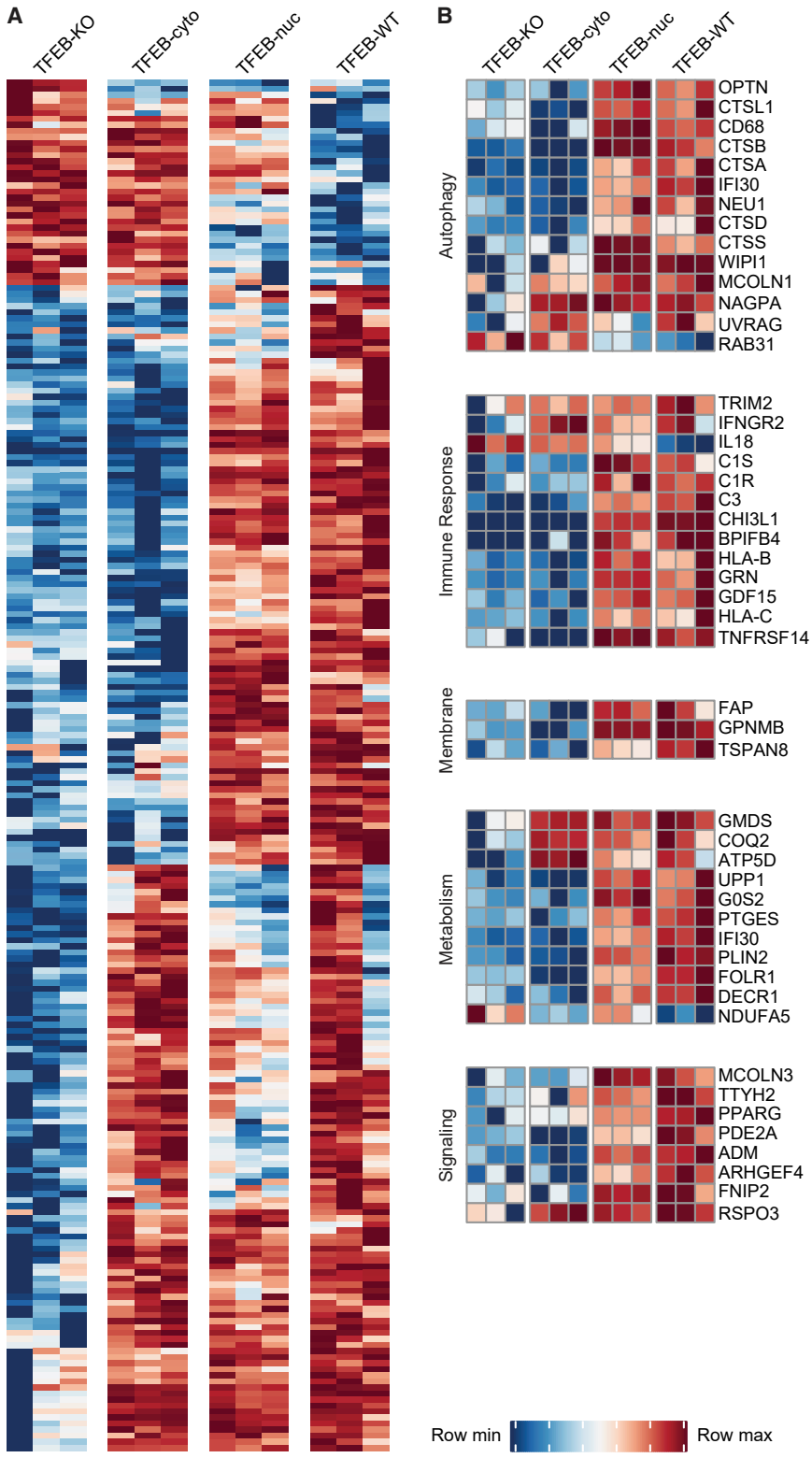

Figure 2. TFEB at Steady State Induces a Transcriptional Response that Is Amplified by Sustained Nuclear Localization

(A) Relative gene expression (CPM-transformed measurements) for genes differentially expressed between TFEB-KO and TFEB-WT cells with fold change (FC) > 1.5 or FC < −1.5 at steady state. Data from three biological replicates for each cell line are shown. For each gene, rows were scaled such that their minimum expression value was 0 and their maximum expression value was 1, and only genes with a relative expression value > 0.7 or a relative expression value < 0.3 in at least 8 of the 12 RNA sequencing samples are shown. Full list in Table S2.

(B) Select genes upregulated in TFEB-WT and TFEB-nuc cells at steady state. See also Figure S2 and Tables S1, S2, and S3.

receptor localized to endosomes (Hastings and Cresswell, 2011; Singh et al., 2008; Ward et al., 2016; Wibowo et al., 2013; Zhang et al., 2017). In addition, we identified upregulation of innate immune response genes, including *C1S* and *C3* complement components; *CD68*, a lysosomal/endosomal-associated transmembrane and lectin binding protein; and *GRN*, which has reported roles in signaling and inflammatory response (Nguyen et al., 2018; Sorbara et al., 2018; Tanaka et al., 2013; Zhou et al., 2015). *GPNMB*, a membrane glycoprotein with recently described anti-inflammatory and neuroprotective functions, was among the top differentially expressed genes in TFEB-WT and TFEB-nuc cells at steady state (Budge et al., 2018; Neal et al., 2018; van der Lienden et al., 2018). Using quantitative PCR (qPCR), we validated expression patterns observed by RNA sequencing for selected genes (*CTSD*, *SQSTM1*, *MCOLN1*, *IL33*, *FAP*, *GPNMB*, *IFI30*, *FOLR1*, and *G0S2*). The highest transcript levels for most genes were observed in TFEB-nuc cells, and higher levels of transcription were detected in TFEB-WT cells than in TFEB-cyto or TFEB-KO cells for all genes (Figure S2). Collectively, these data support the role of TFEB in transcriptional regulation of metabolic processes and highlight its importance in sustaining innate immune responses at steady state.

Gene Ontology (GO) analyses of TFEB upregulated genes ($logFC > ln2$ and $q < 0.05$) supported our observations that genes classified as functioning in immune system processes and regulation of inflammatory responses were enriched in TFEB-nuc cells (Bonferroni adjusted $p < 0.05$; Table S3). Similar genes were enriched in TFEB-WT cells but were not statistically significant (Table S3). No GO enrichment was observed in TFEB-cyto cells (Table S3). These data support our findings that nuclear levels in TFEB-WT cells at steady state are sufficient to activate transcription and sustained nuclear localization in TFEB-nuc cells increases this response.

TFEB Expression and Localization Phenotypically Alter Lysosomal and Mitochondrial Compartments

High-content subcellular imaging has been used to characterize responses to genetic or chemical perturbations. Here, we used Cell Painting as an unbiased, image-based profiling approach to detect phenotypic changes of organelles in response to TFEB localization (Bray et al., 2016). In addition to the fluorescent markers used previously in Cell Painting studies to detect DNA, RNA, endoplasmic reticulum (ER), mitochondria, actin, and Golgi and plasma membrane, we included LysoTracker to image effects on lysosomal compartments as a positive control. From captured images, microscopic features, including intensity, radial distribution, granularity, texture, size, and shape of the subcellular structures, were measured and analyzed with CellProfiler to perform illumination correction, quality control, and measurement extraction (Bray et al., 2016).

Similar to transcriptional clustering, the top two principal components of the Cell Painting data illustrated TFEB-cyto and TFEB-nuc cells morphologically resembled TFEB-KO and TFEB-WT cells, respectively, at steady state (Figure 3A). Clustering by genotype remained consistent following treatment with Torin, indicating that reconstitution of TFEB in KO cells had a greater effect on subcellular morphology than treatment with the exogenous stimulus (Figure 3A). Interestingly, TFEB-cyto cells displayed the largest difference between DMSO and Torin treatments, which may be a result of increased dephosphorylated TFEB in the cytosol in response to Torin relative to DMSO treatment (Figures 1C and 3A). Furthermore, using Morpheus software analysis to depict the microscopic features that distinguished TFEB-KO and TFEB-cyto cells from TFEB-WT and TFEB-nuc cells, we observed that 27 of the top 40 differential features by t test analysis were detected in lysosomal or mitochondrial imaging channels (Figure S3). Studies previously detected changes to lysosomal and mitochondrial morphology and positioning (Mansueto et al., 2017; Sardiello et al., 2009; Willett et al., 2017), as well as lysosomal content (Abu-Remaileh et al., 2017), following TFEB stimulation.

To support the Cell Painting data, we assessed lysosomal size and acidification by imaging TFEB-KO and reconstituted cell lines at steady state with LysoView and DQ-BSA markers. Analyses identified no significant difference in lysosomal size (Figure 3B) but did detect decreased lysosomal acidification in TFEB-KO and TFEB-cyto cells compared with TFEB-WT, TFEB-nuc, and WT HeLa cells (Figure 3C). In addition, using MitoTracker Red, we confirmed differences in mitochondrial area per cell between TFEB cell lines at steady state. Compared with TFEB-WT cells, mitochondrial area was reduced in TFEB-KO and TFEB-cyto cells (Figure 3D). Furthermore, representative confocal images of cells stained with MitoTracker Red illustrate that mitochondria in TFEB-KO and TFEB-cyto cells are concentrated in the perinuclear region rather than distributed throughout the cell (Deus et al., 2020). Our data indicate that steady-state levels of nuclear TFEB activate transcripts capable of inducing detectable phenotypic changes to lysosomal and mitochondrial compartments compared with cells lacking nuclear TFEB.

TFEB Target Genes Are Differentially Sensitive to Nuclear TFEB

Our approach using TFEB-KO cells reconstituted with TFEB-WT or TFEB-nuc enabled an evaluation of the global TFEB-dependent transcriptional response at steady state and after mTOR inhibition. We hypothesized that treatment of TFEB-WT cells with Torin would induce transcription of genes not detected at steady state, because increased nuclear translocation in response to exogenous stimuli would increase accessibility or binding of TFEB to the promoter region of its target genes. In contrast, we predicted there would be no significant transcriptional response in TFEB-nuc cells following Torin treatment, because we showed TFEB is restricted to the nucleus (Figure 1A).

We compared RNA sequencing data from TFEB-WT or TFEB-nuc cells relative to TFEB-KO cells at steady state and following Torin treatment. At steady state, TFEB-WT and TFEB-nuc cells activated transcription, including expected target genes (Figure 1D; Tables S1 and S4), whereas Torin treatment predominantly increased the magnitude of expression in TFEB-WT cells but had no significant transcriptional effect on TFEB-nuc cells (Figures 4A and 4B; Table S4). A direct comparison of differential gene expression between TFEB-WT and TFEB-nuc cells confirmed TFEB-WT cells upregulated these genes in response to Torin, whereas TFEB-nuc cells did not (Figure S4). Transcriptional responses in TFEB-WT and TFEB-nuc cells were

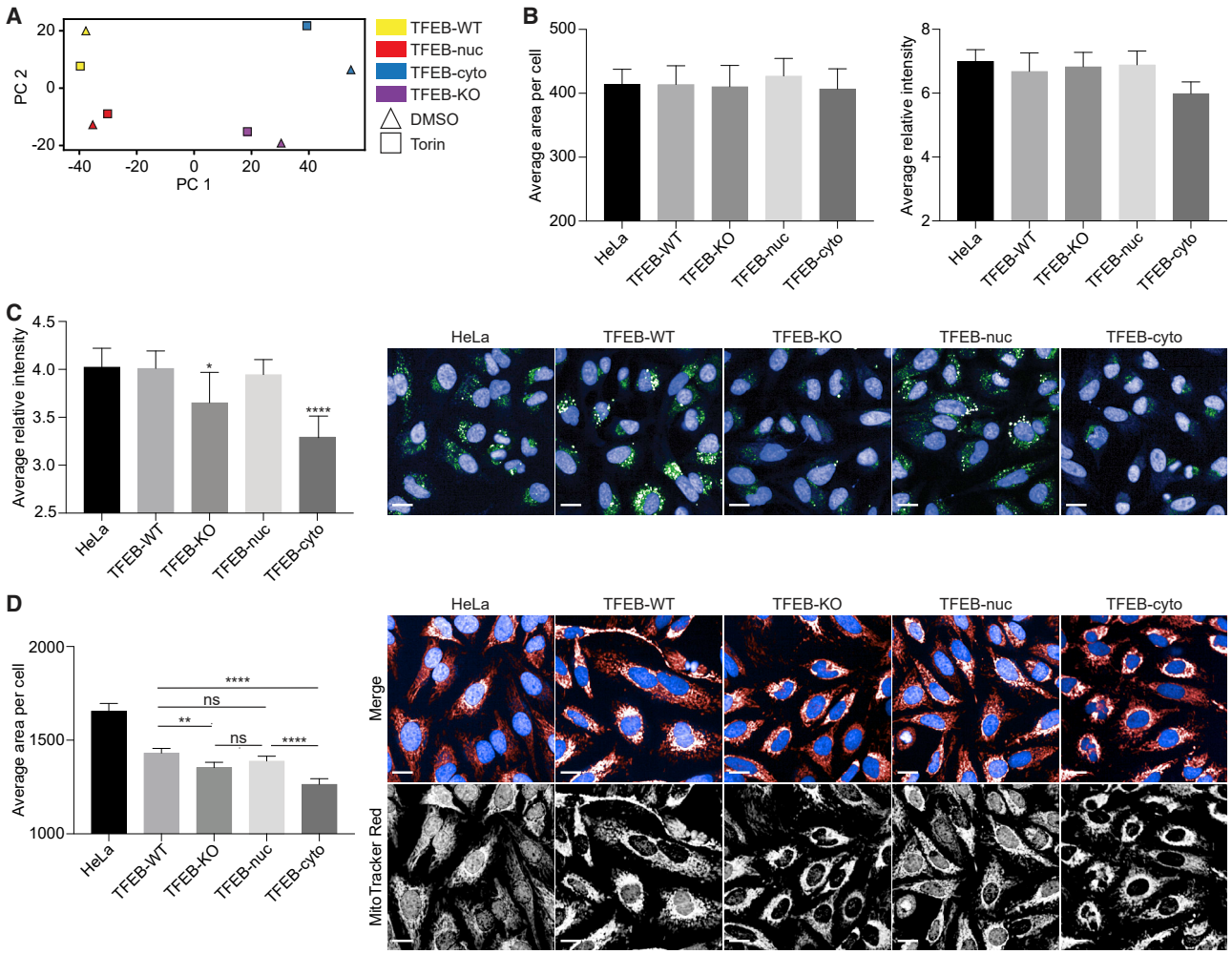

Figure 3. TFEB Expression and Localization Phenotypically Alter Lysosomal and Mitochondrial Compartments

(A) Principal-component analysis (PCA) of Cell Painting subcellular features from TFEB cell lines illustrates that phenotypically TFEB-cyto and TFEB-nuc cells cluster with TFEB-KO and TFEB-WT cells, respectively, following DMSO or Torin treatment.

(B) Quantification of average lysosomal area per cell and relative fluorescence intensity by LysoView staining showed no significant differences among TFEB-KO, reconstituted cell lines, and WT HeLa cells relative to TFEB-WT.

(C) Quantification of average relative intensity of DQ-BSA. Significance values shown are relative to TFEB-WT. In representative confocal images, DNA is detected with Hoechst (blue) and acidified lysosomal compartments by DQ-BSA (green).

(D) Quantification of average mitochondrial area per cell as detected by MitoTracker Red. Significance values are for comparisons as shown. In representative confocal images, DNA is detected with Hoechst (blue in merged channels) and mitochondria with MitoTracker Red (red in merged channels; white in single channels).

For all quantifications, data from at least two independent experiments and at least 500 cells per experiment were analyzed using ordinary one-way ANOVA and Tukey's multiple comparison test with single pooled variance. Data are represented as mean ± SEM. *$p < 0.05$, **$p < 0.01$, ****$p < 0.0001$. ns, not significant. Scale bars represent 5 μm. See also Figure S3.

comparable at steady state (Figures S1C and S4B–S4D). A subset of genes was only upregulated in Torin-treated TFEB-WT cells and was not transcribed at detectable levels in untreated TFEB-WT cells or in TFEB-nuc cells (Figures 4C and 4D; Table S4). Genes responsive to high, sustained levels of nuclear TFEB induced by Torin treatment included *CTSF*, *NPC2*, *BLOC1S3*, and *BLOC1S2*, which function in lysosomal degradation, transport, and biogenesis; *NDUFS4*, *NDUFA13*, *NDUFA8*, *NDUFA1*, *NDUFB10*, and *NDUFAF2*, subunits of mitochondrial NADH dehydrogenase; *PPARG* and *PPARGC1A*, a nuclear receptor and co-factor regulating lipid metabolism; and *BHLHE40* and *BHLHE41*, two transcriptional repressors (Figures 4B and 4D; Table S4).

A subset of TFEB-dependent genes did not respond to Torin stimulation (Figures 4E and 4F; Table S4), including lysosomal proteases (*CTSA*, *CTSB*, *CTSD*, and *CTSS*), lysosomal membrane proteins (*C1orf85*), stress response/tissue repair proteins (*FAP* and *GRN*), and complement components (*C1S*, *C1R*, and *C3*). Upregulation of these genes in TFEB-WT and TFEB-nuc cells irrespective of Torin stimulation suggests that low levels

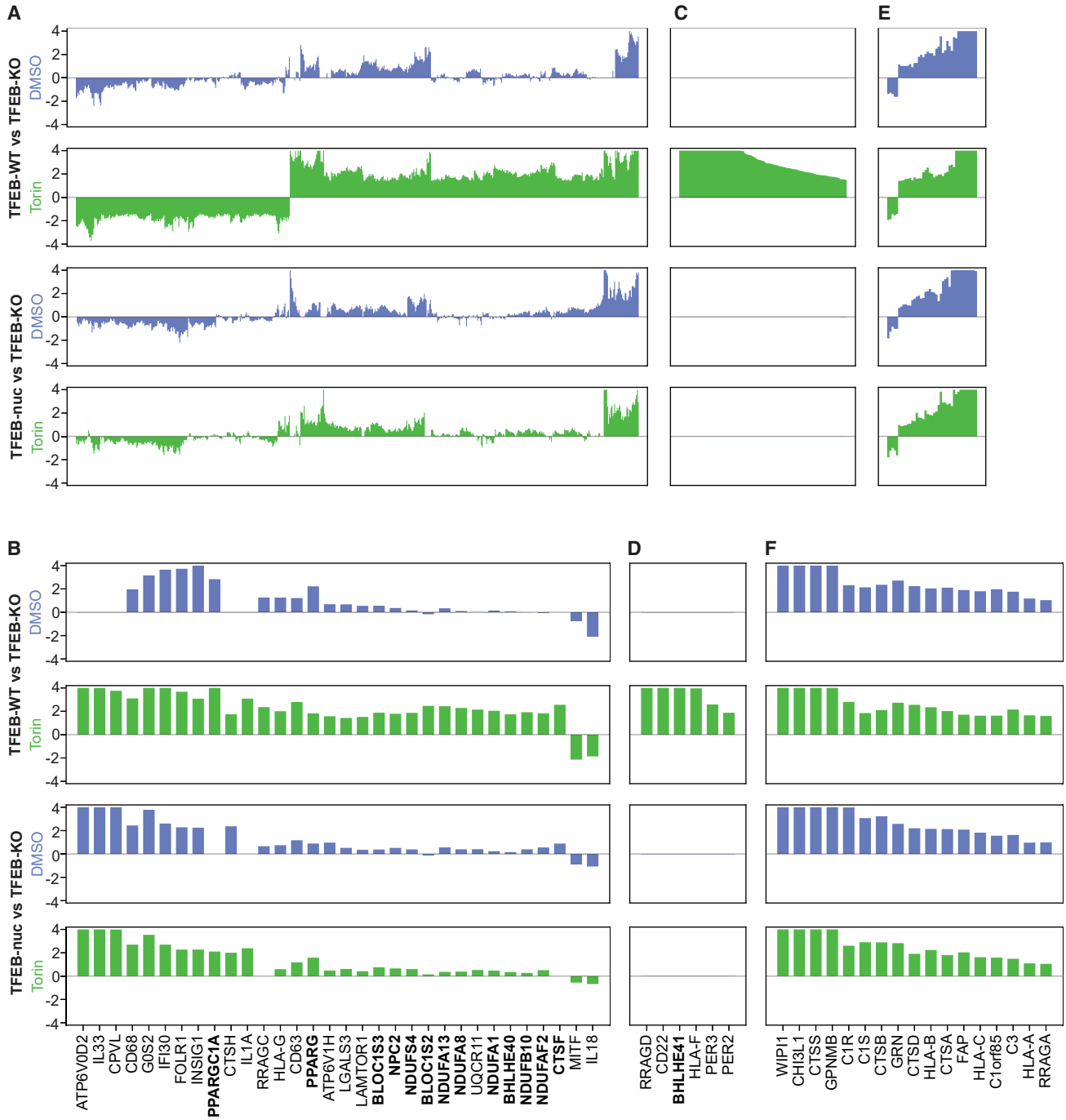

Figure 4. TFEB Target Genes Are Differentially Sensitive to Nuclear TFEB

TFEB-KO, TFEB-WT, and TFEB-nuc cells were treated with Torin or DMSO and then processed for RNA sequencing analysis. Panels show differential gene expression from steady state (DMSO, blue) and Torin-treated (green) TFEB-WT versus TFEB-KO cells and TFEB-nuc versus TFEB-KO cells. Each bar corresponds to a gene, and the y axis represents logFC of differential gene expression (truncated logFC ± ln4). Genes represented in the bar plots are all genes (A, C, and E) or select genes (B, D, and F) with significant differential expression (logFC > ln4 or logFC < −ln4 and q < 0.01) in TFEB-WT relative to TFEB-KO cells following Torin treatment. For each differential expression comparison, (A) and (B) represent genes significantly upregulated with Torin treatment, (C) and (D) represents genes significantly upregulated with Torin treatment yet not transcribed at detectable levels without Torin stimulation, and (E) and (F) represent TFEB-dependent genes for which transcription did not significantly change in response to Torin stimulation. Genes in bold indicate those highlighted in Results. See also Figure S4 and Table S4.

of nuclear TFEB are sufficient to maximally induce their transcription.

TFEB Transcriptional Signature Is Modulated by Different Exogenous Stimuli

Our data show that intracellular *Salmonella* defense requires autophagy and lysosomal pathways, induction of which activates a TFEB transcriptional response (Kuo et al., 2018; Ravenhill et al., 2019; Verlhac et al., 2015; Wang et al., 2018; Figure S5A). To address whether different stimuli activate unique TFEB transcriptional circuits, we examined responses in TFEB-KO and TFEB-WT cells infected with *Salmonella enterica* serovar Typhimurium. Similar to Torin-treated cells (Figures 4 and 5A), infected TFEB-WT cells induced a TFEB-dependent transcriptional response that included many known targets (Figures 5A, S5B, and S5C; Table S1; Sardiello et al., 2009). By comparing stimulus-dependent differential expression patterns, we identified genes that (1) displayed a greater magnitude of transcriptional response following Torin treatment than following *Salmonella* infection (e.g., *CTSF*, *BLOC1S2*, *BLOC1S3*, and *LGALS3*); (2) shared a similar magnitude of transcriptional response following either Torin treatment or *Salmonella* infection (e.g., *CTSS*, *WIPI1*, *C1R*, *C1S*, and *C3*); or (3) were differentially expressed in either Torin-treated or *Salmonella*-infected cells (e.g., *BHLHE40*, *BHLHE41*, and *PER2*) (Figures 5B, 5C, S5B, and S5C).

TFEB-dependent genes upregulated at steady state were identified among those maximally expressed following both Torin treatment and *Salmonella* infection, confirming that these genes require low levels of nuclear TFEB for transcription (Figures 4, 5B, 5C, S5B, and S5C). Based on GO analyses, these genes were enriched in immune response and autophagy pathways (Figures 5D and S5D; Table S5). Enrichment of autophagy genes following Torin treatment and bacterial infection was expected, because both mTOR inhibition and intracellular pathogens are known to induce a TFEB-dependent autophagy response (Li et al., 2018; Murano et al., 2017; Najibi et al., 2016; Napolitano et al., 2018; Roczniak-Ferguson et al., 2012). We also detected *Salmonella*-specific upregulated genes, including genes related to autophagy and lysosomes (*CALCOCO1*, *TBK1*, *DRAM1*, *GNS*, *HPS3*, *HPS4*, and *HPS4*), innate immune response (*BFIFB4*, *IL1B*, *IL24*, and *IL6R*), and phosphoinositide lipid signaling and vesicular trafficking (*MTM1*, *SACM1L*, *ANKFY1*, *GOLPH3L*, *WDFY1*, *WDFY3*, and *COPB2*) (Table S5). These data provide the first evidence linking xenophagy with upregulation of TFEB target genes. When investigating TFEB- and Torin-dependent genes that did not respond to *Salmonella* infection by GO analyses, we identified enrichment in genes functioning in mitochondrial processes (Figures 5E, S5B, and S5D; Table S5), including glutaredoxins and subunits of the NADH:ubiquinone oxidoreductase, cytochrome *c* oxidase, and ubiquinol-cytochrome *c* reductase complexes. These findings suggest that transcriptional regulation of a subset of targets depends on the pathway by which TFEB is activated (Figures 5 and S5; Table S5). Notably, *BHLHE40* and *BHLHE41* were upregulated only in response to Torin treatment, indicating a response to the strength or nature of the stimulus (Figures 5A and S5B).

TFEB Protects and BHLHE40 and BHLHE41 Sensitize Cells to Lysosomal Cell Death

We next sought to determine how TFEB target genes directly influence lysosomal functions. Traditionally thought to function predominantly in cellular degradative processes, lysosomes are viewed as intracellular hubs integrating signals required for both catabolic and anabolic pathways (Lawrence and Zoncu, 2019; Perera and Zoncu, 2016). To identify genes involved in lysosomal functions or regulation, we used L-leucyl-L-leucine methyl ester (LLME) in a genome-wide CRISPR-Cas9 screen. LLME induces lysosomal membrane permeabilization and subsequent cell death by the release of lysosomal enzymes (Repnik et al., 2017; Thiele and Lipsky, 1990). We reasoned that CRISPR-mediated disruption of genes such as cathepsin C (*CTSC*), a lysosomal protease critical for LLME-induced cell death, would protect cells from LLME treatment, whereas disruption of lysosomal biogenesis or cellular homeostasis genes would sensitize cells (Brojatsch et al., 2015; Jacobson et al., 2013). Because of their high levels of lysosomal activity and sensitivity to LLME treatment (Jin et al., 2018), BV2 microglial cells stably expressing Cas9 were transduced with a pooled CRISPR library, followed by treatment with LLME or a mock control. Sequencing data for both positively (protective) and negatively (sensitized) enriched guide RNAs were deconvolved, and STARS score rankings and false discovery rates (FDRs) were determined (Table S6; Doench et al., 2016). Validating our results, *CTSC* was the top-ranked positively enriched gene (Figure 6A; Table S6). *TFEB* was negatively enriched, suggesting that its role in lysosomal biogenesis is required to protect cells from LLME-induced cell death (Figure 6A; Table S6).

To pinpoint additional TFEB-dependent genes functioning in lysosomal biology, we compared the list of genes upregulated in a TFEB- and Torin-dependent manner with the output from the genome-wide CRISPR screen. Several genes were negatively enriched, including ones with higher STARS rankings than *TFEB*: *CSTB*, *NPC2*, *GALE*, *ZMIZ1*, *HECTD1*, *FAM102A*, *SH3BP2*, and *BLOC1S2* (Figure 6B; Table S6). Additional components of the biogenesis of lysosomal organelle complex 1—BLOC1S1, BLOC1S5, and Snapin, which are thought to initiate lysosomal biogenesis (Lee et al., 2012; Luzio et al., 2014)—were among the top 5% of negatively enriched genes by STARS ranking (Table S6). These data indicate that to survive the stress of lysosomal damage inflicted by LLME treatment, cells respond by translocating TFEB into the nucleus and initiating lysosomal biogenesis pathways. TFEB target genes (*BHLHE40*, *BHLHE41*, *RRAGC*, *CASP8*, *SNX27*, *PPM1H*, and *IQCG*) were also among the top 10% of positively enriched genes, indicating that deletion of these genes protects cells from LLME-induced cell death (Figure 6B; Table S6). Although caspase-8 depletion may prevent caspase-dependent cell death upon LLME treatment, the protective roles that other TFEB targets play require further investigation.

BHLHE40 and BHLHE41 Repress Expression of Select TFEB Target Genes through a Negative Feedback Loop

Considering that BHLHE40 and BHLHE41 (1) are TFEB target genes (Palmieri et al., 2011), (2) bind to the same consensus E

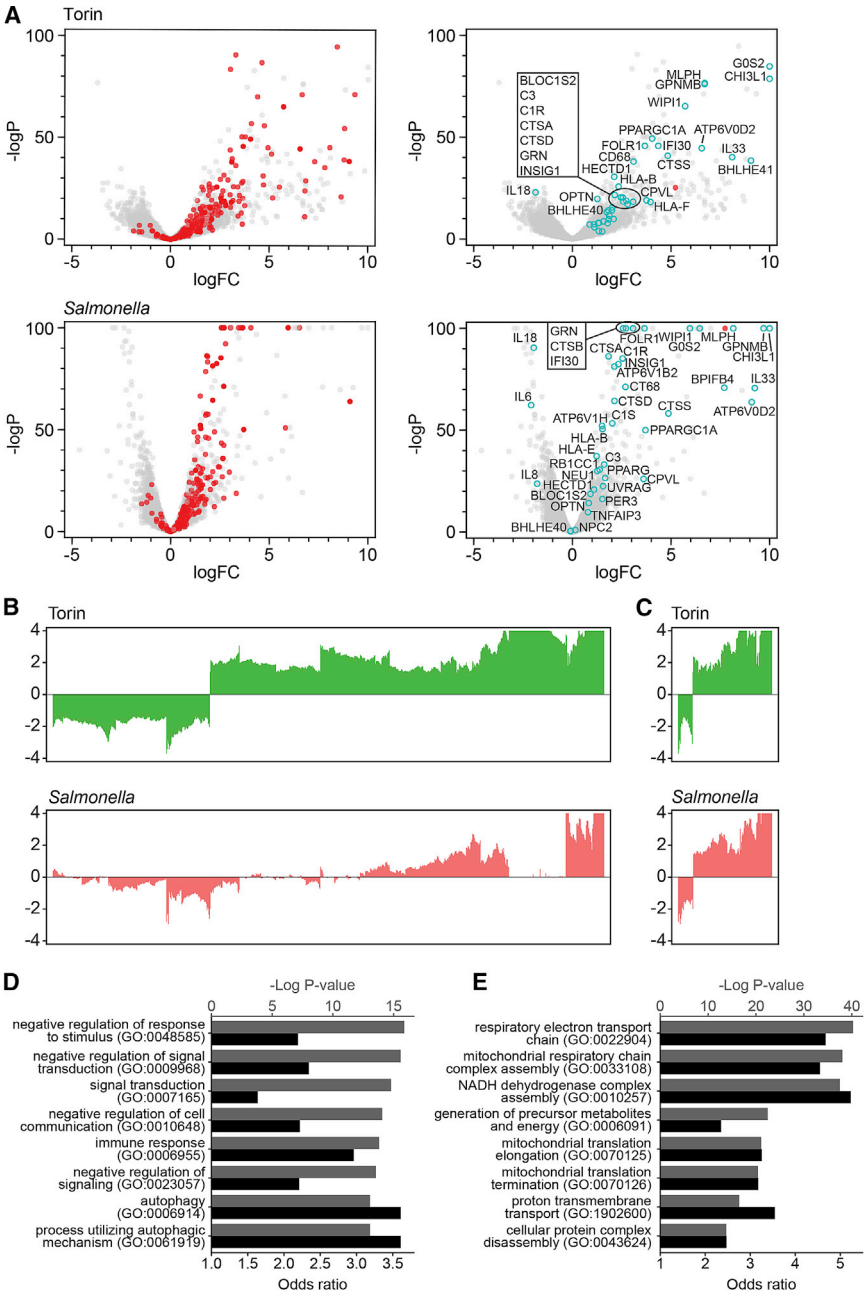

Figure 5. TFEB Transcriptional Signature Is Modulated by Different Exogenous Stimuli

(A) Volcano plots illustrate differential gene expression from TFEB-KO and TFEB-WT cell lines treated with Torin (upper) or infected with *S. enterica* (lower). Genes shown in red in left panels are previously reported TFEB target genes (Table S1: Sardiello et al., 2009), many of which are significantly upregulated in response to both Torin and intracellular bacteria based on logP and logFC. Select genes functioning in autophagy, lysosomal, and immune responses are highlighted in cyan in the right panels. Compared with TFEB-KO cells, TFEB transcript level is significantly increased in response to stimuli, as denoted in red in the right panels.

(B) Comparison of TFEB-dependent transcriptional profiles in response to Torin and *S. enterica* infection. Genes shown are differentially expressed in TFEB-WT versus TFEB-KO cells in response to Torin treatment (logFC > ln4 or logFC < −ln4 and q < 0.01).

(C) Bar plots of genes differentially expressed in response to both Torin treatment and *Salmonella* infection (logFC > ln4 or logFC < −ln4 and q < 0.01).

(D) Gene Ontology enrichment analysis of genes upregulated in response to both Torin and *Salmonella* infection (logFC > ln2 and q < 0.05). Black bars represent −log p values, and gray bars represent odds ratios.

(E) Gene Ontology enrichment analysis of genes upregulated in response to Torin (logFC > ln2 and q < 0.05), but not in response to *Salmonella* (logFC < ln1.5 and q > 0.9). Black bars represent −log p values, and gray bars represent odds ratios. See also Figures 4 and S5 and Tables S1 and S5.

box motif as TFEB (Chung et al., 2015; Kanda et al., 2016; Nakashima et al., 2008; Nishiyama et al., 2012), (3) are only upregulated in response to high levels of nuclear TFEB (Figures 4B and 4D; Table S4), and (4) act in opposition to TFEB in response to lysosomal damage (Figure 6; Table S6), we hypothesized that BHLHE40 and BHLHE41 function as counter-regulators of TFEB target genes through competitive DNA binding in a negative feedback loop. To test this, we used the CRISPR-Cas9 system to generate a BHLHE40/41 double-knockout (dKO) HeLa cell line, which we reconstituted with empty vector (BHLHE40/41-dKO) or with WT BHLHE40 and BHLHE41 (BHLHE40/41-WT). Deletion and reconstitution of the *BHLHE40/41* genes were confirmed by DNA sequencing and immunoblot (Figure S6A). Increases in logFC of *BHLHE40* and *BHLHE41* transcripts in BHLHE40/41-WT relative to BHLHE40/41-dKO cells were observed and served as internal controls for the RNA sequencing data (Figure S6B). Volcano plots representing BHLHE40/41-dependent gene regulation revealed that BHLHE40/41 both induced and repressed gene transcription (Figure 7A)—in contrast to TFEB, which predominantly induced gene transcription (Figure 1D). In addition, the analysis demonstrated that TFEB- and Torin-dependent upregulated genes were both up- and downregulated in response to BHLHE40/41 reconstitution (Figure 7A).

Next, to identify genes upregulated by TFEB and downregulated by BHLHE40/41 in an unbiased manner, we dissected different branches of TFEB-dependent response pathways that are preferentially activated upon different cellular conditions and external stimuli using an unsupervised gene clustering method (t-stochastic neighborhood embedding [tSNE]) on all RNA sequencing datasets in our study. Validating this approach,

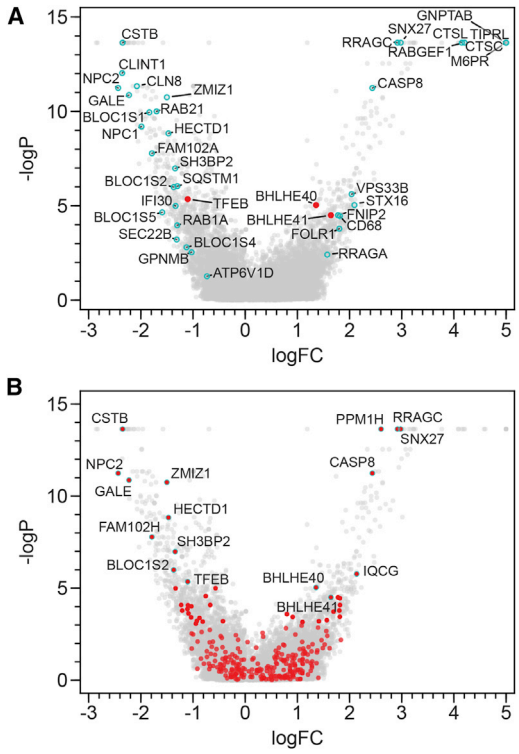

Figure 6. TFEB Protects and BHLHE40 and BHLHE41 Sensitize Cells to Lysosomal Cell Death

Visualization of STARS analysis from a genome-wide CRISPR screen in BV2 cells identifying genes that sensitize cells to (negative logFC) or protect cells from (positive logFC) LLME treatment.

(A) TFEB, BHLHE40, and BHLHE41 (red) and select genes of interest (cyan).

(B) Data from the genome-wide CRISPR screen are shown, with genes in red representing all those found by RNA sequencing to be significantly upregulated in TFEB-WT versus TFEB-KO cells following Torin treatment (logFC > ln4 and q < 0.01). Genes of particular interest are outlined with cyan. See also Table S6.

we successfully recovered known target genes that clustered around TFEB (Figure 7B; Table S1; Sardiello et al., 2009). Moreover, we observed a large cluster of genes that were upregulated in TFEB-WT cells and trended toward downregulation in BHLHE40/41-WT cells following Torin treatment, including genes that we identified as sensitive to low levels of nuclear TFEB (*CTSS*, *PPARGC1A*, *IFI30*, and *GPNMB*) (Figures 4, 7B–7D, S5B, and S5C). Limiting our analysis to the strongest putative competing targets from all genes (logFC > ln2 and logFC < −ln2 in TFEB- and BHLHE40/41-WT versus TFEB- and BHLHE40/41-KO cells, respectively, and q < 0.05 in both) (Figure 7E; Table S7), we searched for their overlap with known motifs in published ChIP-seq datasets with HOMER (Heinz et al., 2010) and found predominantly basic-helix-loop-helix (bHLH) transcription factor binding site enrichment in their promoter regions. Controlling the false discovery only among bHLH transcription factor binding sites highlighted overenrichment of TFE3/TFEB binding motifs (Palmieri et al., 2011; Sardiello et al., 2009) and the overlapping BHLHE40 and BHLHE41 binding motifs (Table S8). Published TFEB, BHLHE40, and BHLHE41 ChIP-seq datasets provided additional evidence that these transcription factors are able to bind promoter regions of competing target genes in cellular contexts (GEO: GSM2354032, Doronzo et al., 2019; GEO: GSE106000, ENCODE Project Consortium, 2012; GEO: GSM2797493 and GSM2461743, Kreslavsky et al., 2017; Table S8).

To confirm the RNA sequencing data and analyses, several of the genes we identified as most significantly upregulated by TFEB and downregulated by BHLHE40/41 were examined by qPCR: transcript levels of *CTSS*, *IFI30*, *INSIG1*, *GPNMB*, and *PPARGC1A* were elevated in TFEB-expressing cells and reduced in BHLHE40/41-expressing cells (Figure 7F). These data validate previously reported TFEB, BHLHE40, and BHLHE41 target genes from ChIP-seq analyses (ENCODE Project Consortium, 2012; Doronzo et al., 2019; Kreslavsky et al., 2017) and identify putative common targets that may be cell type or stimulation specific (Figure 7G; Table S8). Altogether, our data provide evidence for a BHLHE40/41-dependent negative feedback loop not previously described that counter-regulates select TFEB target genes.

DISCUSSION

As a master regulator of essential cellular processes, TFEB affects a range of lysosomal storage, metabolic, neurodegenerative, and cardiac diseases. Here, we used RNA sequencing and genome-wide CRISPR approaches to discover TFEB localization- and stimulus-specific responses. Clustering target genes based on responsiveness to nuclear-localized TFEB and evaluating their effects in response to lysosomal membrane permeabilization revealed a BHLHE40/41-dependent counter-regulatory mechanism capable of downregulating a subset of TFEB targets.

By comparing transcriptional signatures at steady state or after stimulation, we observed that most TFEB-dependent genes were upregulated in response to mTOR inhibition, including known and previously unknown targets, such as mitochondrial respiratory chain complex subunits. These observations indicated that most TFEB targets are induced in response to increased cellular demand and demonstrated that the level of nuclear TFEB titrates the magnitude of transcription, providing an effective mechanism by which cells tightly control responses to cellular stimuli (Kribelbauer et al., 2019). In contrast, we observed that select components of the complement, lysosomal, and autophagy pathways were transcriptionally upregulated at steady state in TFEB-WT cells. The magnitude of expression of these genes did not change in response to nuclear-localized TFEB or Torin treatment, suggesting that their enhancer motif is highly accessible and requires low levels of nuclear TFEB for activation. Furthermore, deficiencies in the lysosomal protease and classical complement component genes are associated with lysosomal storage, neurodegenerative, and autoimmune diseases (Butler et al., 2019; Lintner et al., 2016; Macedo and Isaac, 2016; Marques et al., 2020; Nakajima et al., 2019; Prada et al., 2014; Tang et al., 2006). Thus, cells likely require a constant level of transcription of these innate immune response genes to maintain homeostasis or rapidly respond to exogenous stimuli. Our data illustrate that TFEB

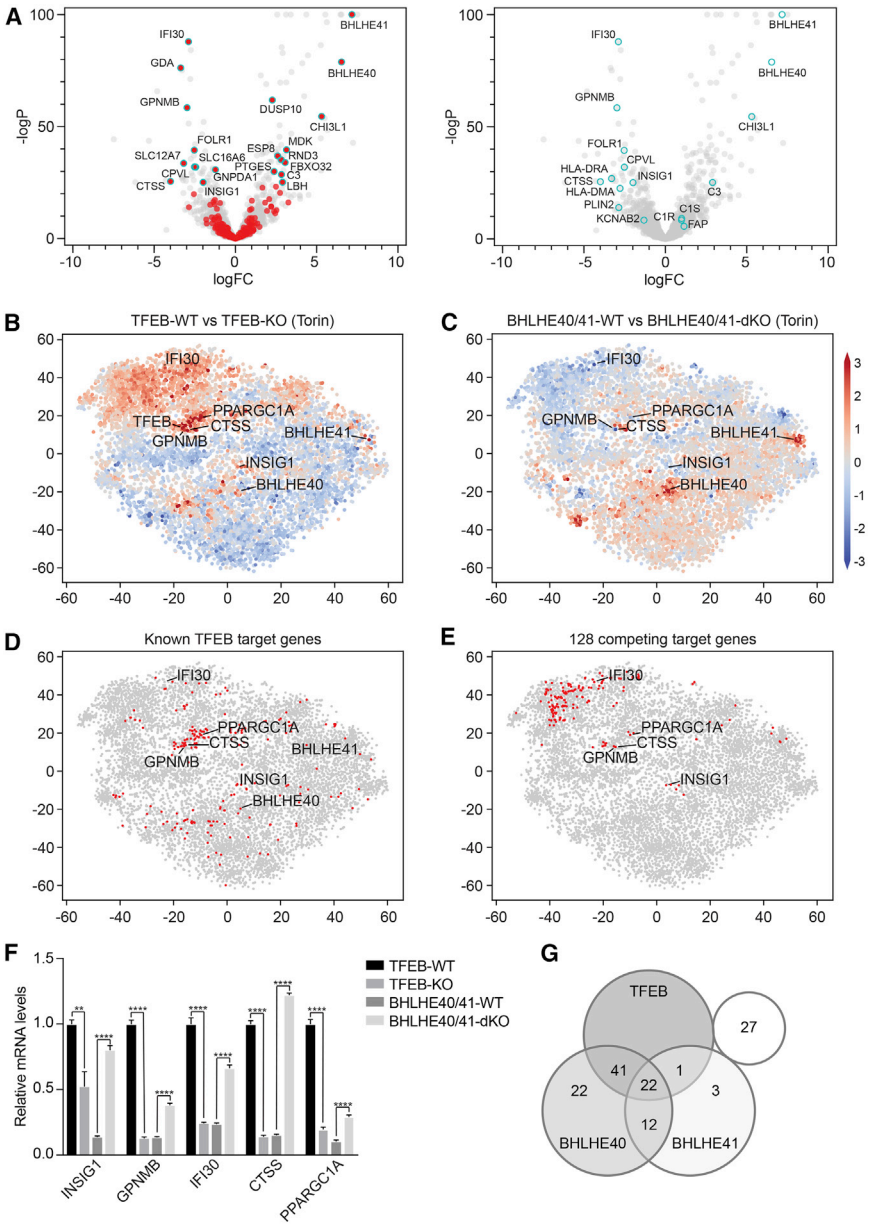

Figure 7. BHLHE40 and BHLHE41 Repress Expression of Select TFEB Target Genes through a Negative Feedback Loop

(A) Volcano plots depicting differential gene expression in BHLHE40/41-WT versus BHLHE40/41-KO cells reconstituted cells at steady state. Highlighted in red (left panel) are genes significantly upregulated in TFEB-WT versus TFEB-KO cells following Torin treatment (logFC > ln4 and q < 0.01). Highlighted in cyan (right panel) are select TFEB target genes.

(B–E) tSNE plots representing all RNA sequencing datasets in our study. Comparison of RNA sequencing datasets from (B) TFEB-WT and TFEB-KO cells or (C) BHLHE40/41-WT and BHLHE40/41-dKO cells treated with Torin, in which each gene (dot) is colored by the logFC. (D) Known TFEB target genes or (E) strongest putative TFEB and BHLHE40/41 competing target genes are highlighted in red.

(F) Gene expression of select TFEB and BHLHE40/41 target genes in TFEB-KO, TFEB-WT, BHLHE40/41-dKO, and BHLHE40/41-WT cells as quantified by qRT-PCR. By two-tailed t test analyses, all genes were significantly upregulated in cells reconstituted with TFEB and downregulated in those reconstituted with BHLHE40/41. Data are representative from three independent experiments (mean ± SEM [standard error of the mean]). **p < 0.006, ****p < 0.0001.

(G) Venn diagram represents the number of the 128 strongest putative competing target genes (logFC > ln2 and < −ln2 in TFEB- and BHLHE40/41-WT versus TFEB- and BHLHE40/41-KO cells, respectively, and q < 0.05 in both) bound by TFEB, BHLHE40, and/or BHLHE41 based on the published ChIP-seq datasets GEO: GSM2354032, GSE106000, GSM2797493, and GSM2461743. See also Figure S6 and Tables S7 and S8.

target genes are regulated on multiple levels to differentiate their responsiveness to the intensity and duration of stimulation.

Little is known about how different stimuli or cellular contexts affect TFEB-dependent transcriptional signatures. We investigated TFEB response to mTOR inhibition and bacterial infection. Although both stimuli induced upregulation of genes in TFEB-WT cells, GO analyses identified common and stimulation-specific transcriptional signatures. This unbiased analysis identified shared upregulation of genes classified as functioning in autophagic processes. Both Torin treatment and *Salmonella* infection induced TFEB-dependent transcriptional regulation of signal transduction and immune response genes, such as tumor necrosis factor alpha (TNF-α)-induced proteins (*TNFAIP3* and *TNFAIP6*), complement components (*C1S*, *C1R*, and *C3*), and interleukin-1 (IL-1) cytokine family members (*IL1α*, *IL1R*, and *IL33*). We also discovered autophagy, lysosomal, and membrane trafficking genes (*CALCOCO1*, *TBK1*, *DRAM1*, *GNS*, *HPS3*, *HPS4*, *HPS4*, *MTM1*, *SACM1L*, *ANKFY1*, *GOLPH3L*, *WDFY1*, *WDFY3*, and *COPB2*) that were specifically upregulated in response to *Salmonella* infection, which provides new insights into host innate response to restrict bacteria and maintain cellular homeostasis through xenophagy (El-Houjeiri et al., 2019; Murano et al., 2017; Visvikis et al., 2014).

The predominant difference observed between stimulation-dependent transcriptional signatures was the activation of mitochondrial genes functioning in oxidative respiration following Torin treatment. The overwhelming number of genes encoded subunits for mitochondrial complexes I, III, and IV of the electron transport chain. These data suggested that Torin-induced TFEB translocation stimulates transcriptional activation of genes required for mitochondrial oxidative phosphorylation to maintain cellular ATP levels, in addition to stimulating mitochondrial biogenesis through peroxisome proliferator-activated receptor

gamma coactivator 1 alpha (PGC1α) induction (Mansueto et al., 2017). TFEB-dependent activation of oxidative phosphorylation genes further establishes a role for TFEB in mitochondrial energy production and metabolic homeostasis (Mansueto et al., 2017). Deficiencies in mitochondrial complex genes have been linked to immune-mediated T cell activation and differentiation (Baixauli et al., 2015; Brady et al., 2018; Mansueto et al., 2017; Nabar and Kehrl, 2017), as well as classical mitochondrial diseases, cancer, and neurodegenerative diseases (Fernández-Mosquera et al., 2017; Lynch et al., 2019). Intracellular bacterial infection is also expected to alter cellular metabolism (Cornejo et al., 2017; Eisenreich et al., 2019). Our data may highlight a cellular context-dependent difference, whereby a nutritional stress response results in intense and rapid TFEB-dependent transcriptional activation. Alternatively, a low steady-state level of transcripts may be sufficient to maintain cellular homeostasis until later time points during an infection as the intracellular bacterial burden increases. Therefore, it is possible that the selective upregulation of mitochondrial oxidative phosphorylation genes could depend on the stimulus, its intensity, or a combination of these factors.

Finally, we discovered evidence suggesting that BHLHE40 and BHLHE41 counteract TFEB transcriptional activation. First, these two genes are significantly upregulated upon mTOR inhibition, suggesting that neither gene is required at steady state. We also noted that neither BHLHE40 nor BHLHE41 was differentially expressed following *Salmonella* infection, which may be a consequence of the pathway by which TFEB is activated or of the intensity of stimulation. Second, TFEB protects and BHLHE40/41 sensitizes cells to LLME-induced cell death. Third, BHLHE40/41-dKO cells showed transcriptional effects opposite to those of TFEB-KO cells. Specifically, transcript levels of select genes were higher in TFEB-WT cells lacking BHLHE40/41 and lower in BHLHE40/41-WT cells lacking TFEB. These data suggest a negative feedback mechanism, whereby BHLHE40 and BHLHE41 transcription is upregulated in response to stimulus-dependent TFEB activation and subsequently represses transcription of select TFEB target genes that influence lysosomal function.

STAR★METHODS

Detailed methods are provided in the online version of this paper and include the following:

- KEY RESOURCES TABLE
- RESOURCE AVAILABILITY
  - Lead contact
  - Materials availability
  - Data and code availability
- EXPERIMENTAL MODEL AND SUBJECT DETAILS
  - Cell lines
  - Vector construction
  - Bacterial strains
- METHOD DETAILS
  - Immunofluorescence microscopy
  - Immunoprecipitation
  - LC3 turnover
  - RNA sequencing sample preparation
  - Quantitative PCR
  - Cell Painting
  - Bacterial replication assay
  - Genome-wide CRISPR knockout screen
- QUANTIFICATION AND STATISTICAL ANALYSIS
  - RNA sequencing analysis
  - Relative gene expression
  - Cell Painting
  - CRISPR screen analysis
  - Gene identifier conversion
  - Gene ontology enrichment
  - TSNE visualization
  - Known motif enrichment

SUPPLEMENTAL INFORMATION

Supplemental Information can be found online at https://doi.org/10.1016/j.celrep.2020.108371.

ACKNOWLEDGMENTS

We thank Dr. Christian Münz (University of Zürich) for the gift of GFP-LC3-CSGW and Dr. Yuanan Lu (University of Hawai'i at Mānoa) for the BV2 cell line, Ariel Lefkovith and Bihua Li for RNA sequencing library generation, Kyle Karhohs for imaging analysis of the Cell Painting data, Mukund Varma and Gautam Goel for the initial RNA sequence analysis, and Theresa Reimels for help with manuscript preparation and editing. This work was supported by National Institutes of Health grants R01 DK097485 (to R.J.X.) and U19 AI109725 and U19 AI142784 (to H.W.V. and R.J.X.) and the Center for the Study of Inflammatory Bowel Disease (P30 DK043351 to R.J.X.). S.S. was supported by R35 GM122547 to Anne E. Carpenter. The genome sequence described and used in this research was derived from a HeLa cell line. Henrietta Lacks, and the HeLa cell line that was established from her tumor cells without her knowledge or consent in 1951, have made significant contributions to scientific progress and advances in human health. We are grateful to Lacks, now deceased, and to her surviving family members for their contributions to biomedical research.

AUTHOR CONTRIBUTIONS

Conceptualization, K.L.C., G.L.C.P., K.G.L., and R.J.X.; Investigation, K.L.C., G.L.C.P., D.R.B., J.W.L., P.B., and I.C.F.; Formal Analysis, L.W., L.K., N.R., S.S., and M.K.-A.; Writing—Original Draft, K.L.C., G.L.C.P., L.W., and K.G.L.; Writing—Reviewing and Editing, K.L.C., K.G.L., and R.J.X.; Visualization, K.L.C. and L.W.; Funding Acquisition, H.W.V., and R.J.X.; Supervision, B.N., H.W.V., and R.J.X.

DECLARATION OF INTERESTS

P.B., N.R., and B.N. are employees of Novartis. D.R.B. and H.W.V. are employees of Vir Biotechnology. R.J.X. is a consultant to Novartis and a cofounder of Jnana Therapeutics and Celsius Therapeutics. H.W.V. is a founder of Casma Therapeutics and PierianDx. These organizations did not participate in funding this work.

Received: February 12, 2020
Revised: August 18, 2020
Accepted: October 20, 2020
Published: November 10, 2020

REFERENCES

Abu-Remaileh, M., Wyant, G.A., Kim, C., Laqtom, N.N., Abbasi, M., Chan, S.H., Freinkman, E., and Sabatini, D.M. (2017). Lysosomal metabolomics

reveals V-ATPase- and mTOR-dependent regulation of amino acid efflux from lysosomes. Science *358*, 807–813.

Anders, S., Pyl, P.T., and Huber, W. (2015). HTSeq—a Python framework to work with high-throughput sequencing data. Bioinformatics *31*, 166–169.

Baixauli, F., Acín-Pérez, R., Villarroya-Beltrí, C., Mazzeo, C., Nuñez-Andrade, N., Gabandé-Rodriguez, E., Ledesma, M.D., Blázquez, A., Martin, M.A., Falcón-Pérez, J.M., et al. (2015). Mitochondrial Respiration Controls Lysosomal Function during Inflammatory T Cell Responses. Cell Metab. *22*, 485–498.

Brady, O.A., Martina, J.A., and Puertollano, R. (2018). Emerging roles for TFEB in the immune response and inflammation. Autophagy *14*, 181–189.

Bray, M.A., Fraser, A.N., Hasaka, T.P., and Carpenter, A.E. (2012). Workflow and metrics for image quality control in large-scale high-content screens. J. Biomol. Screen. *17*, 266–274.

Bray, M.A., Singh, S., Han, H., Davis, C.T., Borgeson, B., Hartland, C., Kost-Alimova, M., Gustafsdottir, S.M., Gibson, C.C., and Carpenter, A.E. (2016). Cell Painting, a high-content image-based assay for morphological profiling using multiplexed fluorescent dyes. Nat. Protoc. *11*, 1757–1774.

Brojatsch, J., Lima, H., Jr., Palliser, D., Jacobson, L.S., Muehlbauer, S.M., Furtado, R., Goldman, D.L., Lisanti, M.P., and Chandran, K. (2015). Distinct cathepsins control necrotic cell death mediated by pyroptosis inducers and lysosome-destabilizing agents. Cell Cycle *14*, 964–972.

Budge, K.M., Neal, M.L., Richardson, J.R., and Safadi, F.F. (2018). Glycoprotein NMB: an Emerging Role in Neurodegenerative Disease. Mol. Neurobiol. *55*, 5167–5176.

Butler, V.J., Cortopassi, W.A., Argouarch, A.R., Ivry, S.L., Craik, C.S., Jacobson, M.P., and Kao, A.W. (2019). Progranulin Stimulates the *In Vitro* Maturation of Pro-Cathepsin D at Acidic pH. J. Mol. Biol. *431*, 1038–1047.

Carpenter, A.E., Jones, T.R., Lamprecht, M.R., Clarke, C., Kang, I.H., Friman, O., Guertin, D.A., Chang, J.H., Lindquist, R.A., Moffat, J., et al. (2006). CellProfiler: image analysis software for identifying and quantifying cell phenotypes. Genome Biol. *7*, R100.

Chung, N., Zhang, X.D., Kreamer, A., Locco, L., Kuan, P.F., Bartz, S., Linsley, P.S., Ferrer, M., and Strulovici, B. (2008). Median absolute deviation to improve hit selection for genome-scale RNAi screens. J. Biomol. Screen. *13*, 149–158.

Chung, S.Y., Kao, C.H., Villarroya, F., Chang, H.Y., Chang, H.C., Hsiao, S.P., Liou, G.G., and Chen, S.L. (2015). Bhlhe40 Represses PGC-1α Activity on Metabolic Gene Promoters in Myogenic Cells. Mol. Cell. Biol. *35*, 2518–2529.

Conway, K.L., Kuballa, P., Song, J.H., Patel, K.K., Castoreno, A.B., Yilmaz, O.H., Jijon, H.B., Zhang, M., Aldrich, L.N., Villablanca, E.J., et al. (2013). Atg16l1 is required for autophagy in intestinal epithelial cells and protection of mice from *Salmonella* infection. Gastroenterology *145*, 1347–1357.

Cornejo, E., Schlaermann, P., and Mukherjee, S. (2017). How to rewire the host cell: A home improvement guide for intracellular bacteria. J. Cell Biol. *216*, 3931–3948.

Deus, C.M., Yambire, K.F., Oliveira, P.J., and Raimundo, N. (2020). Mitochondria-Lysosome Crosstalk: From Physiology to Neurodegeneration. Trends Mol. Med. *26*, 71–88.

Doench, J.G., Fusi, N., Sullender, M., Hegde, M., Vaimberg, E.W., Donovan, K.F., Smith, I., Tothova, Z., Wilen, C., Orchard, R., et al. (2016). Optimized sgRNA design to maximize activity and minimize off-target effects of CRISPR-Cas9. Nat. Biotechnol. *34*, 184–191.

Doronzo, G., Astanina, E., Corà, D., Chiabotto, G., Comunanza, V., Noghero, A., Neri, F., Puliafito, A., Primo, L., Spampanato, C., et al. (2019). TFEB controls vascular development by regulating the proliferation of endothelial cells. EMBO J. *38*, e98250.

Eichner, L.J., Brun, S.N., Herzig, S., Young, N.P., Curtis, S.D., Shackelford, D.B., Shokhirev, M.N., Leblanc, M., Vera, L.I., Hutchins, A., Ross, D.S., et al. (2019). Genetic Analysis Reveals AMPK Is Required to Support Tumor Growth in Murine Kras-Dependent Lung Cancer Models. Cell Metab. *29*, 285–302.

Eisenreich, W., Rudel, T., Heesemann, J., and Goebel, W. (2019). How Viral and Intracellular Bacterial Pathogens Reprogram the Metabolism of Host Cells to Allow Their Intracellular Replication. Front. Cell. Infect. Microbiol. *9*, 42.

El-Houjeiri, L., Possik, E., Vijayaraghavan, T., Paquette, M., Martina, J.A., Kazan, J.M., Ma, E.H., Jones, R., Blanchette, P., Puertollano, R., et al. (2019). The Transcription Factors TFEB and TFE3 Link the FLCN-AMPK Signaling Axis to Innate Immune Response and Pathogen Resistance. Cell Rep. *26*, 3613–3628.

ENCODE Project Consortium (2012). An integrated encyclopedia of DNA elements in the human genome. Nature *489*, 57–74.

Fernández-Mosquera, L., Diogo, C.V., Yambire, K.F., Santos, G.L., Luna Sánchez, M., Bénit, P., Rustin, P., Lopez, L.C., Milosevic, I., and Raimundo, N. (2017). Acute and chronic mitochondrial respiratory chain deficiency differentially regulate lysosomal biogenesis. Sci. Rep. *7*, 45076.

Goodman, R.P., Calvo, S.E., and Mootha, V.K. (2018). Spatiotemporal compartmentalization of hepatic NADH and NADPH metabolism. J. Biol. Chem. *293*, 7508–7516.

Hastings, K.T., and Cresswell, P. (2011). Disulfide reduction in the endocytic pathway: immunological functions of gamma-interferon-inducible lysosomal thiol reductase. Antioxid. Redox Signal. *15*, 657–668.

Heinz, S., Benner, C., Spann, N., Bertolino, E., Lin, Y.C., Laslo, P., Cheng, J.X., Murre, C., Singh, H., and Glass, C.K. (2010). Simple combinations of lineage-determining transcription factors prime *cis*-regulatory elements required for macrophage and B cell identities. Mol. Cell *38*, 576–589.

Jacobson, L.S., Lima, H., Jr., Goldberg, M.F., Gocheva, V., Tsiperson, V., Sutterwala, F.S., Joyce, J.A., Gapp, B.V., Blomen, V.A., Chandran, K., et al. (2013). Cathepsin-mediated necrosis controls the adaptive immune response by Th2 (T helper type 2)-associated adjuvants. J. Biol. Chem. *288*, 7481–7491.

Jin, M.M., Wang, F., Qi, D., Liu, W.W., Gu, C., Mao, C.J., Yang, Y.P., Zhao, Z., Hu, L.F., and Liu, C.F. (2018). A Critical Role of Autophagy in Regulating Microglia Polarization in Neurodegeneration. Front. Aging Neurosci. *10*, 378.

Kanda, M., Yamanaka, H., Kojo, S., Usui, Y., Honda, H., Sotomaru, Y., Harada, M., Taniguchi, M., Suzuki, N., Atsumi, T., et al. (2016). Transcriptional regulator Bhlhe40 works as a cofactor of T-bet in the regulation of IFN-γ production in iNKT cells. Proc. Natl. Acad. Sci. USA *113*, E3394–E3402.

Kim, D., Pertea, G., Trapnell, C., Pimentel, H., Kelley, R., and Salzberg, S.L. (2013). TopHat2: accurate alignment of transcriptomes in the presence of insertions, deletions and gene fusions. Genome Biol. *14*, R36.

Klopfenstein, D.V., Zhang, L., Pedersen, B.S., Ramírez, F., Warwick Vesztrocy, A., Naldi, A., Mungall, C.J., Yunes, J.M., Botvinnik, O., Weigel, M., et al. (2018). GOATOOLS: A Python library for Gene Ontology analyses. Sci. Rep. *8*, 10872.

Kreslavsky, T., Vilagos, B., Tagoh, H., Poliakova, D.K., Schwickert, T.A., Wöhner, M., Jaritz, M., Weiss, S., Taneja, R., Rossner, M.J., and Busslinger, M. (2017). Essential role for the transcription factor Bhlhe41 in regulating the development, self-renewal and BCR repertoire of B-1a cells. Nat. Immunol. *18*, 442–455.

Kribelbauer, J.F., Rastogi, C., Bussemaker, H.J., and Mann, R.S. (2019). Low-Affinity Binding Sites and the Transcription Factor Specificity Paradox in Eukaryotes. Annu. Rev. Cell Dev. Biol. *35*, 357–379.

Kuo, C.J., Hansen, M., and Troemel, E. (2018). Autophagy and innate immunity: Insights from invertebrate model organisms. Autophagy *14*, 233–242.

Lawrence, R.E., and Zoncu, R. (2019). The lysosome as a cellular centre for signalling, metabolism and quality control. Nat. Cell Biol. *21*, 133–142.

Lee, H.H., Nemecek, D., Schindler, C., Smith, W.J., Ghirlando, R., Steven, A.C., Bonifacino, J.S., and Hurley, J.H. (2012). Assembly and architecture of biogenesis of lysosome-related organelles complex-1 (BLOC-1). J. Biol. Chem. *287*, 5882–5890.

Li, L., Friedrichsen, H.J., Andrews, S., Picaud, S., Volpon, L., Ngeow, K., Berridge, G., Fischer, R., Borden, K.L.B., Filippakopoulos, P., and Goding, C.R. (2018). A TFEB nuclear export signal integrates amino acid supply and glucose availability. Nat. Commun. *9*, 2685.

Lintner, K.E., Wu, Y.L., Yang, Y., Spencer, C.H., Hauptmann, G., Hebert, L.A., Atkinson, J.P., and Yu, C.Y. (2016). Early Components of the Complement Classical Activation Pathway in Human Systemic Autoimmune Diseases. Front. Immunol. *7*, 36.

Luzio, J.P., Hackmann, Y., Dieckmann, N.M., and Griffiths, G.M. (2014). The biogenesis of lysosomes and lysosome-related organelles. Cold Spring Harb. Perspect. Biol. *6*, a016840.

Lynch, M.R., Tran, M.T., Ralto, K.M., Zsengeller, Z.K., Raman, V., Bhasin, S.S., Sun, N., Chen, X., Brown, D., Rovira, I.I., et al. (2019). TFEB-driven lysosomal biogenesis is pivotal for PGC1α-dependent renal stress resistance. JCI Insight *5*, e126749.

Macedo, A.C., and Isaac, L. (2016). Systemic Lupus Erythematosus and Deficiencies of Early Components of the Complement Classical Pathway. Front. Immunol. *7*, 55.

Mansueto, G., Armani, A., Viscomi, C., D'Orsi, L., De Cegli, R., Polishchuk, E.V., Lamperti, C., Di Meo, I., Romanello, V., Marchet, S., et al. (2017). Transcription Factor EB Controls Metabolic Flexibility during Exercise. Cell Metab. *25*, 182–196.

Marques, A.R.A., Di Spiezio, A., Thießen, N., Schmidt, L., Grötzinger, J., Lüllmann-Rauch, R., Damme, M., Storck, S.E., Pietrzik, C.U., Fogh, J., et al. (2020). Enzyme replacement therapy with recombinant pro-CTSD (cathepsin D) corrects defective proteolysis and autophagy in neuronal ceroid lipofuscinosis. Autophagy *16*, 811–825.

Martina, J.A., and Puertollano, R. (2018). Protein phosphatase 2A stimulates activation of TFEB and TFE3 transcription factors in response to oxidative stress. J. Biol. Chem. *293*, 12525–12534.

Martina, J.A., Chen, Y., Gucek, M., and Puertollano, R. (2012). MTORC1 functions as a transcriptional regulator of autophagy by preventing nuclear transport of TFEB. Autophagy *8*, 903–914.

Martina, J.A., Diab, H.I., Li, H., and Puertollano, R. (2014). Novel roles for the MiTF/TFE family of transcription factors in organelle biogenesis, nutrient sensing, and energy homeostasis. Cell. Mol. Life Sci. *71*, 2483–2497.

Meireles, A.M., Shen, K., Zoupi, L., Iyer, H., Bouchard, E.L., Williams, A., and Talbot, W.S. (2018). The Lysosomal Transcription Factor TFEB Represses Myelination Downstream of the Rag-Ragulator Complex. Dev. Cell *47*, 319–330.

Murano, T., Najibi, M., Paulus, G.L.C., Adiliaghdam, F., Valencia-Guerrero, A., Selig, M., Wang, X., Jeffrey, K., Xavier, R.J., Lassen, K.G., and Irazoqui, J.E. (2017). Transcription factor TFEB cell-autonomously modulates susceptibility to intestinal epithelial cell injury *in vivo*. Sci. Rep. *7*, 13938.

Nabar, N.R., and Kehrl, J.H. (2017). The Transcription Factor EB Links Cellular Stress to the Immune Response. Yale J. Biol. Med. *90*, 301–315.

Najibi, M., Labed, S.A., Visvikis, O., and Irazoqui, J.E. (2016). An Evolutionarily Conserved PLC-PKD-TFEB Pathway for Host Defense. Cell Rep. *15*, 1728–1742.

Nakajima, H., Ueno, M., Adachi, K., Nanba, E., Narita, A., Tsukimoto, J., Itoh, K., and Kawakami, A. (2019). A new heterozygous compound mutation in the *CTSA* gene in galactosialidosis. Hum. Genome Var. *6*, 22.

Nakashima, A., Kawamoto, T., Honda, K.K., Ueshima, T., Noshiro, M., Iwata, T., Fujimoto, K., Kubo, H., Honma, S., Yorioka, N., et al. (2008). DEC1 modulates the circadian phase of clock gene expression. Mol. Cell. Biol. *28*, 4080–4092.

Napolitano, G., Esposito, A., Choi, H., Matarese, M., Benedetti, V., Di Malta, C., Monfregola, J., Medina, D.L., Lippincott-Schwartz, J., and Ballabio, A. (2018). mTOR-dependent phosphorylation controls TFEB nuclear export. Nat. Commun. *9*, 3312.

Neal, M.L., Boyle, A.M., Budge, K.M., Safadi, F.F., and Richardson, J.R. (2018). The glycoprotein GPNMB attenuates astrocyte inflammatory responses through the CD44 receptor. J. Neuroinflammation *15*, 73.

Nguyen, A.D., Nguyen, T.A., Zhang, J., Devireddy, S., Zhou, P., Karydas, A.M., Xu, X., Miller, B.L., Rigo, F., Ferguson, S.M., et al. (2018). Murine knockin model for progranulin-deficient frontotemporal dementia with nonsense-mediated mRNA decay. Proc. Natl. Acad. Sci. USA *115*, E2849–E2858.

Nishiyama, Y., Goda, N., Kanai, M., Niwa, D., Osanai, K., Yamamoto, Y., Senoo-Matsuda, N., Johnson, R.S., Miura, S., Kabe, Y., and Suematsu, M. (2012). HIF-1α induction suppresses excessive lipid accumulation in alcoholic fatty liver in mice. J. Hepatol. *56*, 441–447.

Orchard, R.C., Wilen, C.B., Doench, J.G., Baldridge, M.T., McCune, B.T., Lee, Y.C., Lee, S., Pruett-Miller, S.M., Nelson, C.A., Fremont, D.H., and Virgin, H.W. (2016). Discovery of a proteinaceous cellular receptor for a norovirus. Science *353*, 933–936.

Orvedahl, A., McAllaster, M.R., Sansone, A., Dunlap, B.F., Desai, C., Wang, Y.T., Balce, D.R., Luke, C.J., Lee, S., Orchard, R.C., et al. (2019). Autophagy genes in myeloid cells counteract IFNγ-induced TNF-mediated cell death and fatal TNF-induced shock. Proc. Natl. Acad. Sci. USA *116*, 16497–16506.

Palmieri, M., Impey, S., Kang, H., di Ronza, A., Pelz, C., Sardiello, M., and Ballabio, A. (2011). Characterization of the CLEAR network reveals an integrated control of cellular clearance pathways. Hum. Mol. Genet. *20*, 3852–3866.

Perera, R.M., and Zoncu, R. (2016). The Lysosome as a Regulatory Hub. Annu. Rev. Cell Dev. Biol. *32*, 223–253.

Picelli, S., Björklund, A.K., Faridani, O.R., Sagasser, S., Winberg, G., and Sandberg, R. (2013). Smart-seq2 for sensitive full-length transcriptome profiling in single cells. Nat. Methods *10*, 1096–1098.

Prada, C.E., Gonzaga-Jauregui, C., Tannenbaum, R., Penney, S., Lupski, J.R., Hopkin, R.J., and Sutton, V.R. (2014). Clinical utility of whole-exome sequencing in rare diseases: Galactosialidosis. Eur. J. Med. Genet. *57*, 339–344.

Puertollano, R., Ferguson, S.M., Brugarolas, J., and Ballabio, A. (2018). The complex relationship between TFEB transcription factor phosphorylation and subcellular localization. EMBO J. *37*, e98804.

Rabinowitz, J.D., and White, E. (2010). Autophagy and metabolism. Science *330*, 1344–1348.

Ran, F.A., Hsu, P.D., Wright, J., Agarwala, V., Scott, D.A., and Zhang, F. (2013). Genome engineering using the CRISPR-Cas9 system. Nat. Protoc. *8*, 2281–2308.

Ravenhill, B.J., Boyle, K.B., Von Muhlinen, N., Ellison, C.J., Masson, G.R., Otten, E.G., Foeglein, A., Williams, R., and Randow, F. (2019). The Cargo Receptor NDP52 Initiates Selective Autophagy by Recruiting the ULK Complex to Cytosol-Invading Bacteria. Mol. Cell *74*, 320–329.

Repnik, U., Borg Distefano, M., Speth, M.T., Ng, M.Y.W., Progida, C., Hoflack, B., Gruenberg, J., and Griffiths, G. (2017). L-leucyl-L-leucine methyl ester does not release cysteine cathepsins to the cytosol but inactivates them in transiently permeabilized lysosomes. J. Cell Sci. *130*, 3124–3140.

Rioux, J.D., Xavier, R.J., Taylor, K.D., Silverberg, M.S., Goyette, P., Huett, A., Green, T., Kuballa, P., Barmada, M.M., Datta, L.W., et al. (2007). Genome-wide association study identifies new susceptibility loci for Crohn disease and implicates autophagy in disease pathogenesis. Nat. Genet. *39*, 596–604.

Robinson, M.D., McCarthy, D.J., and Smyth, G.K. (2010). edgeR: a Bioconductor package for differential expression analysis of digital gene expression data. Bioinformatics *26*, 139–140.

Roczniak-Ferguson, A., Petit, C.S., Froehlich, F., Qian, S., Ky, J., Angarola, B., Walther, T.C., and Ferguson, S.M. (2012). The transcription factor TFEB links mTORC1 signaling to transcriptional control of lysosome homeostasis. Sci. Signal. *5*, ra42.

Rusmini, P., Cortese, K., Crippa, V., Cristofani, R., Cicardi, M.E., Ferrari, V., Vezzoli, G., Tedesco, B., Meroni, M., Messi, E., et al. (2019). Trehalose induces autophagy via lysosomal-mediated TFEB activation in models of motoneuron degeneration. Autophagy *15*, 631–651.

Sanjana, N.E., Shalem, O., and Zhang, F. (2014). Improved vectors and genome-wide libraries for CRISPR screening. Nat. Methods *11*, 783–784.

Sardiello, M., Palmieri, M., di Ronza, A., Medina, D.L., Valenza, M., Gennarino, V.A., Di Malta, C., Donaudy, F., Embrione, V., Polishchuk, R.S., et al. (2009). A gene network regulating lysosomal biogenesis and function. Science *325*, 473–477.

Settembre, C., Di Malta, C., Polito, V.A., Garcia Arencibia, M., Vetrini, F., Erdin, S., Erdin, S.U., Huynh, T., Medina, D., Colella, P., et al. (2011). TFEB links autophagy to lysosomal biogenesis. Science *332*, 1429–1433.

Settembre, C., Zoncu, R., Medina, D.L., Vetrini, F., Erdin, S., Erdin, S., Huynh, T., Ferron, M., Karsenty, G., Vellard, M.C., et al. (2012). A lysosome-to-nucleus

signalling mechanism senses and regulates the lysosome via mTOR and TFEB. EMBO J. *31*, 1095–1108.

Settembre, C., De Cegli, R., Mansueto, G., Saha, P.K., Vetrini, F., Visvikis, O., Huynh, T., Carissimo, A., Palmer, D., Klisch, T.J., et al. (2013). TFEB controls cellular lipid metabolism through a starvation-induced autoregulatory loop. Nat. Cell Biol. *15*, 647–658.

Silvestrini, M.J., Johnson, J.R., Kumar, A.V., Thakurta, T.G., Blais, K., Neill, Z.A., Marion, S.W., St Amand, V., Reenan, R.A., and Lapierre, L.R. (2018). Nuclear Export Inhibition Enhances HLH-30/TFEB Activity, Autophagy, and Lifespan. Cell Rep. *23*, 1915–1921.

Singh, R., and Cuervo, A.M. (2011). Autophagy in the cellular energetic balance. Cell Metab. *13*, 495–504.

Singh, R., Jamieson, A., and Cresswell, P. (2008). GILT is a critical host factor for *Listeria monocytogenes* infection. Nature *455*, 1244–1247.

Sorbara, M.T., Foerster, E.G., Tsalikis, J., Abdel-Nour, M., Mangiapane, J., Sirluck-Schroeder, I., Tattoli, I., Van Dalen, R., Isenman, D.E., Rohde, J.R., et al. (2018). Complement C3 Drives Autophagy-Dependent Restriction of Cyto-invasive Bacteria. Cell Host Microbe *23*, 644–652.

Tan, H.W.S., Anjum, B., Shen, H.M., Ghosh, S., Yen, P.M., and Sinha, R.A. (2019). Lysosomal inhibition attenuates peroxisomal gene transcription via suppression of PPARA and PPARGC1A levels. Autophagy *15*, 1455–1459.

Tanaka, Y., Matsuwaki, T., Yamanouchi, K., and Nishihara, M. (2013). Increased lysosomal biogenesis in activated microglia and exacerbated neuronal damage after traumatic brain injury in progranulin-deficient mice. Neuroscience *250*, 8–19.

Tang, C.H., Lee, J.W., Galvez, M.G., Robillard, L., Mole, S.E., and Chapman, H.A. (2006). Murine cathepsin F deficiency causes neuronal lipofuscinosis and late-onset neurological disease. Mol. Cell. Biol. *26*, 2309–2316.

Thiele, D.L., and Lipsky, P.E. (1990). Mechanism of L-leucyl-L-leucine methyl ester-mediated killing of cytotoxic lymphocytes: dependence on a lysosomal thiol protease, dipeptidyl peptidase I, that is enriched in these cells. Proc. Natl. Acad. Sci. USA *87*, 83–87.

van der Lienden, M.J.C., Gaspar, P., Boot, R., Aerts, J.M.F.G., and van Eijk, M. (2018). Glycoprotein Non-Metastatic Protein B: An Emerging Biomarker for Lysosomal Dysfunction in Macrophages. Int. J. Mol. Sci. *20*, 66.

Verlhac, P., Viret, C., and Faure, M. (2015). Handcuffs for bacteria—NDP52 orchestrates xenophagy of intracellular *Salmonella*. Microb. Cell *2*, 214–215.

Visvikis, O., Ihuegbu, N., Labed, S.A., Luhachack, L.G., Alves, A.F., Wollenberg, A.C., Stuart, L.M., Stormo, G.D., and Irazoqui, J.E. (2014). Innate host defense requires TFEB-mediated transcription of cytoprotective and antimicrobial genes. Immunity *40*, 896–909.

Wang, L., Yan, J., Niu, H., Huang, R., and Wu, S. (2018). Autophagy and Ubiquitination in *Salmonella* Infection and the Related Inflammatory Responses. Front. Cell. Infect. Microbiol. *8*, 78.

Ward, C., Martinez-Lopez, N., Otten, E.G., Carroll, B., Maetzel, D., Singh, R., Sarkar, S., and Korolchuk, V.I. (2016). Autophagy, lipophagy and lysosomal lipid storage disorders. Biochim. Biophys. Acta *1861*, 269–284.

Wibowo, A.S., Singh, M., Reeder, K.M., Carter, J.J., Kovach, A.R., Meng, W., Ratnam, M., Zhang, F., and Dann, C.E., 3rd. (2013). Structures of human folate receptors reveal biological trafficking states and diversity in folate and antifolate recognition. Proc. Natl. Acad. Sci. USA *110*, 15180–15188.

Willett, R., Martina, J.A., Zewe, J.P., Wills, R., Hammond, G.R.V., and Puertollano, R. (2017). TFEB regulates lysosomal positioning by modulating TMEM55B expression and JIP4 recruitment to lysosomes. Nat. Commun. *8*, 1580.

Xin, J., Mark, A., Afrasiabi, C., Tsueng, G., Juchler, M., Gopal, N., Stupp, G.S., Putman, T.E., Ainscough, B.J., Griffith, O.L., et al. (2016). High-performance web services for querying gene and variant annotation. Genome Biol. *17*, 91.

Xu, Y., Ren, J., He, X., Chen, H., Wei, T., and Feng, W. (2019). YWHA/14-3-3 proteins recognize phosphorylated TFEB by a noncanonical mode for controlling TFEB cytoplasmic localization. Autophagy *15*, 1017–1030.

Zhang, X., Heckmann, B.L., Campbell, L.E., and Liu, J. (2017). G0S2: A small giant controller of lipolysis and adipose-liver fatty acid flux. Biochim. Biophys. Acta Mol. Cell Biol. Lipids *1862* (*10 Pt B*), 1146–1154.

Zhou, X., Sun, L., Bastos de Oliveira, F., Qi, X., Brown, W.J., Smolka, M.B., Sun, Y., and Hu, F. (2015). Prosaposin facilitates sortilin-independent lysosomal trafficking of progranulin. J. Cell Biol. *210*, 991–1002.

STAR★METHODS

KEY RESOURCES TABLE

REAGENT or RESOURCE	SOURCE	IDENTIFIER
Antibodies		
Mouse anti-FLAG	Cell Signaling Technology	Cat #2368S; RRID: AB_2217020
Phospho-(ser) 14-3-3 binding motif	Cell Signaling Technology	Cat #9601S; RRID: AB_330306
Goat anti-mouse IgG	Thermo Fisher	Cat #A11029; RRID: AB_138404
Pan 14-3-3	Santa Cruz	Cat #SC-133233; RRID: AB_2016726
Monoclonal anti-β-actin	Millipore Sigma	Cat #A1978; RRID: AB_476692
Monoclonal anti-FLAG M2	Millipore Sigma	Cat #F3165; RRID: AB_259529
Rabbit anti-LC3B	Millipore Sigma	Cat #L7543; RRID: AB_796155
Bacterial and Virus Strains		
S. Typhimurium SL1344 Xen26	Conway et al., 2013	N/A
S. Typhimurium SL1344 DsRed2	Rioux et al., 2007	N/A
Chemicals, Peptides, and Recombinant Proteins		
Torin-1	Millipore Sigma	Cat #475991
Paraformaldehyde	Electron Microscopy Sciences	Cat #15714
LysoView 488	Biotium	Cat #70067-T
DQ-BSA	Thermo Fisher	Cat #D12051
MitoTracker Red	Thermo Fisher	Cat #M22415
MitoTracker Deep Red	Thermo Fisher	Cat #M22426
Concanavalin A, Alexa Fluor 488 Conjugate	Thermo Fisher	Cat #C11252
SYTO14 green fluorescent nucleic acid stain	Thermo Fisher	Cat #S7576
Wheat Germ Agglutinin, Alexa Fluor 647 Conjugate	Thermo Fisher	Cat # W32466
Alexa Fluor 594 Phalloidin	Thermo Fisher	Cat #A12381
LysoTracker Deep Red	Thermo Fisher	Cat #L12492
L-Leucyl-L-Leucyl methyl ester (LLME)	Cayman Chemicals	Cat #16008
Critical Commercial Assays		
Strep-Tactin Sepharose resin	IBA Life Sciences	Cat #2-1201-010
Agencourt AMPure XP beads	Beckman Coulter	Cat #A63881
Nextera XT DNA Library Prep Kit	Illumina	Cat #FC-131-1096
Nextera XT Index Kit	Illumina	Cat #TG-131-2001
Zymoclean gel DNA recovery column	Zymo Research Corp	Cat #D4008
iScript cDNA Synthesis Kit	Bio-Rad	Cat #1708891
iQ SYBR Green Supermix Kit	Bio-Rad	Cat # 1708884
RNeasy Plus Mini Kit	QIAGEN	Cat #74136
DNeasy Blood and Tissue Kit	QIAGEN	Cat #69506
Deposited Data		
RNA-seq data, see Table S2	Submitted to dbGaP	phs002099
Experimental Models: Cell Lines		
Human: HeLa	ATCC	Cat #CCL-2
Human: HeLa TFEB-KO	This paper	N/A
Human: HeLa TFEB-WT	This paper	N/A
Human: HeLa TFEB-cyto	This paper	N/A
Human: HeLa TFEB-nuc	This paper	N/A
Human: HeLa BHLHE40/BHLHE41 dKO	This paper	N/A

(*Continued on next page*)

Continued

REAGENT or RESOURCE	SOURCE	IDENTIFIER
Human: HeLa BHLHE40/41 dKO/BHLHE40/41 WT	This paper	N/A
Murine: BV-2	Laboratory of Yuanan Lu	N/A
Oligonucleotides		
qPCR primers	This paper	See Table S2
Recombinant DNA		
GFP-LC3-CGSW	Laboratory of Christian Münz	N/A
EGFP-N1-TFEB	Roczniak-Ferguson et al., 2012	Addgene #38119
BHLHE40 Human Tagged ORF clone	OriGene	RC210294L1
BHLHE41 Human Tagged ORF clone	OriGene	RC206882L1
lentiCRISPR v2	Ran et al., 2013	Addgene #52961
lentiCas9-Blast	Sanjana et al., 2014	Addgene #52962
Mouse sgRNA library Brie in lentiCRISPRv2	Doench et al., 2016	Addgene #73632
Software and Algorithms		
NIS-Elements	Nikon	N/A
Harmony High-Content Imaging and Analysis Software	Perkin Elmer	N/A
CellProfiler software version 2.1.0	Carpenter et al., 2006	https://cellprofiler.org/
Morpheus	https://software.broadinstitute.org/morpheus	N/A
STARS software	Doench et al., 2016	https://portals.broadinstitute.org/gpp/public/software/stars
Mygene 3.1.0	Xin et al., 2016	https://pypi.org/project/mygene/
Goatools	Klopfenstein et al., 2018	https://github.com/tanghaibao/goatools
HOMER	Heinz et al., 2010	http://homer.ucsd.edu/homer/
GraphPad Prism8	GraphPad Software, Inc.	N/A

RESOURCE AVAILABILITY

Lead contact

Further information and requests for resources and reagents should be directed to and will be fulfilled by the Lead Contact, Ramnik J. Xavier (xavier@molbio.mgh.harvard.edu).

Materials availability

Materials generated in this study will be provided upon request.

Data and code availability

The accession number for the RNA sequencing data reported in this paper is database of Genotypes and Phenotypes (dbGaP) HeLa Cell Genome Sequencing Studies: phs002099 and listed in Table S2.

EXPERIMENTAL MODEL AND SUBJECT DETAILS

Cell lines

HeLa cells were cultured in Iscove's Modified Dulbecco's Medium supplemented with GlutaMAX, 10% Fetal Bovine Serum and 15 μg/ml gentamicin. TFEB-KO HeLa cells were generated by targeting exons 1, 4 and 5 of the coding region with TFEB-sgRNA 20-nucleotide guide sequences in the lentiCRISPR v2 backbone (Ran et al., 2013) and transducing low-passage HeLa cells. Two days post-transduction, cells were placed under selection with 2 μg/ml of puromycin, and 4-days post-transduction, single cell clones were generated by limiting dilution in 96-well plates. Similarly, double knockouts of BHLHE40 and BHLHE41 were generated by simultaneously targeting exon 1 of BHLHE40 and exon 3 of BHLHE41 with sgRNA guides. Clones were screened for successful knockout via western blot and Sanger sequencing.

Vector construction

To complement the knockout cells, lentivirus was made based on N-terminal Flag-StrepII-tagged CSGW-T2A-blasticidin (TFEB and BHLHE41; GFP-LC3-CSGW backbone was a generous gift from Dr. Christian Münz, University of Zürich) or N-terminal CSGW-T2A-puromycin (BHLHE40) backbones. TFEB cDNA was sub-cloned out of EGFP-N1-TFEB (Roczniak-Ferguson et al., 2012). The TFEB nuclear localized mutant (TFEB-nuc) was made by deleting the first 30 amino acids of the protein sequence containing the lysosomal targeting sequence (Roczniak-Ferguson et al., 2012), and the TFEB cytoplasmic mutant (TFEB-cyto) was generated by mutating basic residues found within the predicted nuclear localization signal (R245-R248) to alanine residues, as previously described (Roczniak-Ferguson et al., 2012). BHLHE40 and BHLHE41 were subcloned from OriGene's RC210294L1 and RC206882L1 plasmids into the CSGW backbones. In addition to reconstituting the BHLHE40/41 double knockout cell line with BHLHE40 and BHLHE41, the double knockout and reconstituted lines were transduced with TFEB-WT and corresponding empty vector to induce higher levels of TFEB induced transcription. After reconstitution with empty vector, wild-type or mutant cDNA, cells were cultured under selection (2 μg/ml puromycin and/or 5 μg/ml blasticidin). When cells were plated for experiments, they were plated in the absence of antibiotics (bacterial or mammalian).

Bacterial strains

Salmonella enterica serovar Typhimurium strain SL1344 expressing the *Photorhabdus luminescens lux* operon (Xen26) (Conway et al., 2013) and *S.* Typhimurium SL1344 DsRed2 (Rioux et al., 2007) were grown on Luria-Bertani (LB) agar or in LB media containing 30 μg/ml kanamycin.

METHOD DETAILS

Immunofluorescence microscopy

Cells were seeded onto 18mm glass coverslips in 12-well plates. The following day, cells were treated with DMSO or 2 μM Torin-1 for 3 h prior to processing for microscopy. Briefly, cells were washed with phosphate buffered saline (PBS) then fixed for 15min at RT with PBS containing 4% (v/v) paraformaldehyde. After fixation, cells were washed with PBS, blocked and permeabilized for 1 h with PBS containing 5% (v/v) goat serum and 0.1% (v/v) Triton X-100 then incubated overnight at 4°C in PBS containing 5% (v/v) goat serum and mouse anti-FLAG antibody (1/1000). The following day, cells were washed with PBS, incubated for 1 h at RT with goat anti-mouse secondary antibody then washed and mounted on glass slides. Confocal images were captured with an Andor Zyla 4.2 plus digital camera at 40× using a Nikon Ti2-E inverted microscope with W1 spinning disk confocal and Nikon NIS-Elements. For LysoView 488, DQ-BSA or MitoTracker Red, cells were stained as per manufacturer's instructions, and live confocal images were captured using a Perkin Elmer Opera Phenix system equipped with a high NA 20x air objective and Perkin Elmer Harmony High-Content Imaging and Analysis Software.

Immunoprecipitation

TFEB knockout HeLa cells reconstituted with empty vector (TFEB-KO), TFEB-WT or TFEB-cyto were seeded into 10cm dishes. The following day, cells were treated with DMSO or 2 μM Torin-1 for 2 h prior to scraping cells and lysing on ice for 30min. Lysate was centrifuged for 15min at 4°C. From the supernatant, an input sample was collected, treated with 6× sample buffer, boiled, and stored at −20°C. To immunoprecipitate TFEB, the remainder of the supernatant was transferred to a tube containing pre-washed Strep-Tactin Sepharose resin and incubated on a rotator for 2 h at 4°C. Resin was washed three times with lysis buffer before boiling in 1x sample buffer. The input and immunoprecipitated samples were separated by SDS-Page, transferred to PVDF and detected by immunoblot with antibodies recognizing the Phospho-(ser) 14-3-3 binding motif (1/1000), anti-FLAG M2 epitope (1/1000) and Pan 14-3-3 (1/100). β-actin served as a loading control (1/1000).

LC3 turnover

TFEB knockout HeLa cells reconstituted with empty vector (TFEB-KO), TFEB-WT, TFEB-cyto, or TFEB-nuc were seeded in 24-well plates at 6 x10^4 cells/well. The following day, cells were treated with 2 μM Torin-1 ± 10 μg/mL E64d/Pepstatin A for 6 h at 37°C. Cells were washed and lysed with RIPA buffer containing protease inhibitor cocktail on ice for 30min. Prior to SDS-PAGE, protein concentrations were determined by BCA assay. Equal amounts of protein samples were loaded and separated by 4%–20% bis-tris SDS-PAGE gel, transferred onto PVDF membranes and detected by immunoblot with rabbit anti-LC3B (1/1000). β-actin to serve as a loading control.

RNA sequencing sample preparation

TFEB and BHLHE40/41 cell lines were seeded in 12-well plates at 1.5x10^5 cells/well or 24-well plates at 7.5x10^4 cells/well, respectively. The following day, cells were treated with DMSO (6 h), 2 μM Torin-1 (6 h) or infected with *S.* Typhimurium SL1344 DsRed2 (MOI 200:1; 6 h). After treatment, TFEB and BHLHE40/41 cells were lysed in 400 μL or 150 μL TCL-buffer (QIAGEN) containing 1% (v/v) beta-mercaptoethanol, respectively, and stored at −80°C until sequenced.

Full-length cDNA libraries were prepared with lysate from approximately 200 cells per sample with a modified version of the SmartSeq2 protocol previously described (Picelli et al., 2013). Post SmartSeq2, double stranded cDNA was purified with Agencourt AMPure XP beads and tagged using the Nextera XT DNA Library Prep Kit and the Nextera XT index kit. Post reaction purification was

performed with Agencourt AMPure XP beads. The samples were pooled, and size selection was performed by gel extraction with Zymoclean gel DNA recovery column after a 2% E-Gel EX Agarose Gel. Samples were prepared and loaded onto a NextSeq 500 (Illumina) per the manufacturer's instructions.

Quantitative PCR

Total RNA was extracted using RNeasy Plus Mini Kit after which cDNA was generated by reverse transcription using the iSCRIPT cDNA synthesis kit according to manufacturer's instructions. Real-time PCR was performed with gene specific primers using the iQ SYBR Green Supermix kit as per manufacturer's instructions. Relative mRNA abundance was calculated with the ΔΔCt method where samples were normalized to GAPDH or B2M.

Cell Painting

TFEB-KO, TFEB-WT, TFEB-nuc and TFEB-cyto HeLa cells were plated at a density of 1,500 cells/well in a 384-well plate (Perkin Elmer; 384 CellCarrier Ultra Microplate) with 6 replicates per plate 48 h prior to staining. Cell Painting procedure followed the previously published protocol (Bray et al., 2016). Briefly, nine different cell components and organelles were stained with fluorescent dyes: nucleus, endoplasmic reticulum (concanavalin A/AlexaFluor488 conjugate), nucleoli and cytoplasmic RNA (SYTO14 green fluorescent nucleic acid stain), Golgi apparatus and plasma membrane (wheat germ agglutinin/AlexaFluor594 conjugate), F-actin (phalloidin/AlexaFluor594 conjugate) and mitochondria (MitoTracker Deep Red) or lysosomes (LysoTracker Deep Red). WGA and MitoTracker/LysoTracker were added to living cells, with the remaining stains carried out after cell fixation with PBS containing 3.2% (v/v) formaldehyde. Images from five fluorescent channels were captured at 20x magnification on an Opera Phenix High Content Screening System (Perkin Elmer): DAPI (387/447 nm), GFP (472/520 nm), Cy3 (531/593 nm), Texas Red (562/624 nm), Cy5 (628/692 nm). Nine sites per well were acquired, with laser based autofocus using the DAPI channel at the first site of each well.

Bacterial replication assay

Cells were plated in 96-well plates at a density of $1.5x10^4$ cells/well in antibiotic-free media 18 h prior to infection (8 replicates per condition). An overnight culture of bioluminescent *S.* Typhimurium SL1344 Xen26 was subcultured for 4 h and then diluted 1:200 in antibiotic-free media for infection of the cells. After a 30min infection, plates were washed 4 times with IMDM media containing 10% (v/v) FBS and 50 μg/ml gentamycin. At 2 h post-infection, culture media was replaced with IMDM media containing 10% FBS and 20 μg/ml gentamycin. Luciferase counts per second were read every hour from 2–10 h post-infection using a PerkinElmer TopCount NXT. Fold replication was calculated at each time point per well.

Genome-wide CRISPR knockout screen

The microglia-like cell line BV2 (kindly provided by Dr. Yuanan Lu, University of Hawai'i at Mānoa) stably expressing Cas9 (Addgene, 52962; Sanjana et al., 2014) was transduced with the Brie mouse CRISPR knockout library (Addgene, 73632; Doench et al., 2016) as previously described (Orchard et al., 2016). For the L-Leucyl-L-Leucine methyl ester (LLME) challenge, 500 cells per guide were plated in duplicate for each treatment condition and after 16 h were treated with 2.5mM LLME or DMSO for mock condition. After 24 h treatment, cells were washed with growth media and new media was added. Surviving cells were allowed to propagate over the next 7 days. Cells were harvested, re-plated then re-challenged with 2.5mM LLME. Cells were washed with growth media after 24 h treatment and new media was added. Surviving cells were allowed to propagate over the next 48 h. Cells were harvested and DNA was isolated using the DNeasy Blood & Tissue Kit according to manufacturer's instructions.

QUANTIFICATION AND STATISTICAL ANALYSIS

All statistical analyses not described in detail below were performed and visualized using GraphPad Prism8. Descriptions of statistical tests used, number of replicates, mean and SEM can be found in figure legends.

RNA sequencing analysis

After sequencing, reads were aligned to the human reference genome hg19 using Tophat2 (Kim et al., 2013). Htseq-count (Anders et al., 2015) summarized read counts for each gene, and R/Bioconductor packages edgeR (Robinson et al., 2010) was used for differential expression (DE) analysis. Differential gene expression determined using edgeR was restricted to genes with average counts per million (CPM) values greater than 1 in at least one of the two conditions compared. p values were obtained from edgeR. FDR and q-value for the remaining genes were calculated using Benjamini-Hochberg procedure. Differential gene expression thresholds can be found in the figure legends.

Relative gene expression

The relative expression was calculated from the $\log_2$ CPM-transformed measurements. Specifically, for each gene, $\log_2$ CPMs were scaled such that their minimum expression value was 0 and maximum value was 1. Only genes with relative expression values > 0.7 or < 0.3 in 8 of the 12 RNA sequencing samples were included in the analysis. The hierarchical clustering was done in pheatmap using the complete linkage with Euclidean distance (default settings).

Cell Painting

Workflow for image processing and cellular feature extraction has been previously described (Bray et al., 2016). In summary, CellProfiler (Carpenter et al., 2006) software version 2.1.0 was used to correct the image channels for uneven illumination, and identify, segment, and measure the cells. An image quality workflow (Bray et al., 2012) was applied to exclude saturated and/or out of focus wells. Cellular morphological, intensity, textural, and adjacency statistics were then measured for the cell, nuclei, and cytoplasmic sub-compartments. Details for the complete list of features and their meaning can be found here: https://github.com/carpenterlab/2016_bray_natprot/wiki/What-do-Cell-Painting-features-mean%3F

Cellular features extracted were normalized as follows: for each feature, the median and median absolute deviation were calculated across all untreated cells within a plate; feature values for all the cells in the plate were then normalized by subtracting the median and dividing by the median absolute deviation (MAD) times 1.4826 (Chung et al., 2008). Features having MAD = 0 in any plate were excluded. Morpheus was used to visualize and analyze the data (https://software.broadinstitute.org/morpheus).

Principal components analysis was completed by first removing cell painting features with single or missing values. After averaging wells for each cell line and stimulation, each feature was normalized to zero mean and unit variance. The top 2 principal components were obtained using sklearn.

CRISPR screen analysis

Illumina sequencing and data deconvolution was performed at the Broad Institute as previously described (Orchard et al., 2016). For analysis, read counts were log-normalized for each guide using the following formula: log-normalized reads per million for guide = $\log_2$((# of reads for guide / total reads in condition x 1e6) +1). Log-normalized reads were averaged for each sample, and untreated average was subtracted from LLME treated average to achieve the $\log_2$ fold changes for each sgRNA, which were then averaged to gene-level $\log_2$ fold changes (https://github.com/mhegde/volcano_plots) as previously described (Table S6) (Orvedahl et al., 2019). The STARS program (https://portals.broadinstitute.org/gpp/public/software/stars) was used to obtain gene-level p values (Table S6) (Doench et al., 2016).

Gene identifier conversion

Mygene was used to convert gene identifiers between identifier systems (Xin et al., 2016). One-to-many maps/conversions are resolved as follows: we regarded two gene identifiers in any identifier system(s) as the same gene if their converted ensembl IDs have any overlap. For enrichment analyses, all converted identifiers are included (in background or test sets).

Gene ontology enrichment

Gene names were converted into uniprot IDs, then goatools (Klopfenstein et al., 2018) was used to compute gene ontology enrichment and to obtain Bonferroni adjusted p values. Enrichments with Bonferroni adjusted p values < 0.05 are shown. Background genes are limited to those expressed (average CPM $>= 1$) in either TFEB knockout or reconstituted cells in Torin-1 treatment. As described in figure legends, GO enrichment is defined as logFC $>$ ln2 and q-value < 0.05.

TSNE visualization

From all genes across all TFEB knockout and reconstituted (including overexpression) conditions and all BHLHE40/41 conditions, across all stimulation (DMSO, Torin-1 or *Salmonella*) and all replicates, we removed low expressing genes (CPM < 1 in over 80% of all samples). Log CPM of each gene was normalized to zero mean and unit variance across samples. We performed tSNE dimension reduction on the top 20 principal components of every gene using sklearn.

Known motif enrichment

HOMER analysis (Heinz et al., 2010) was used to compute known motif enrichment and to obtain enrichment p values. Background genes were limited to those expressed (average CPM $>= 1$) in at least one of the four conditions (TFEB knockout or reconstituted, or BHLHE40/41 knockout or reconstituted cells) in Torin-1 treatment. For bHLH-specific q-values, only motifs with "bHLH" annotations were selected to re-run for a separate FDR control.

Cell Reports, Volume *33*

Supplemental Information

TFEB Transcriptional Responses Reveal Negative Feedback by BHLHE40 and BHLHE41

Kimberly L. Carey, Geraldine L.C. Paulus, Lingfei Wang, Dale R. Balce, Jessica W. Luo, Phil Bergman, Ianina C. Ferder, Lingjia Kong, Nicole Renaud, Shantanu Singh, Maria Kost-Alimova, Beat Nyfeler, Kara G. Lassen, Herbert W. Virgin, and Ramnik J. Xavier

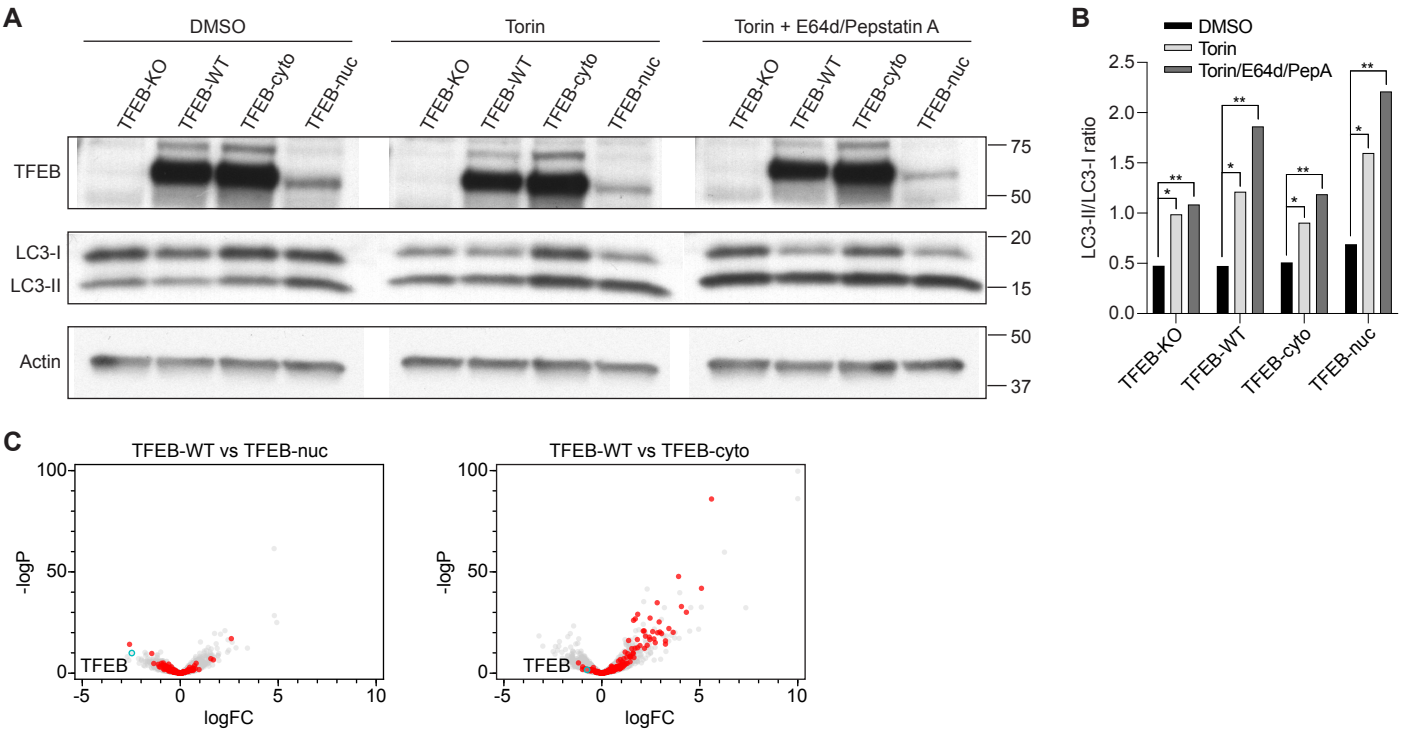

Figure S1. TFEB nuclear translocation is necessary for robust autophagy induction and transcriptional response. Related to Figure 1. Representative immunoblot **(A)** and quantification **(B)** of LC3 conversion in TFEB-KO and reconstituted HeLa cell lines treated with DMSO (0.1%), Torin (1μM), or a combination of Torin and E64d/Pepstatin A for 4hrs. Quantification of LC3-II/LC3-I ratio was normalized to actin loading control. Data are representative of three independent experiments and were analyzed using ordinary two-way ANOVA and Tukey's multiple comparisons test with individual variances for each comparison. Data are represented as mean +/- SEM (standard error of the mean). *p<0.05, **p<0.01. **C)** Cells were processed for RNA sequencing. Transcriptional responses to TFEB expression and localization are shown in volcano plots, where TFEB transcript is shown in cyan and a subset of known TFEB target genes (Table S1) (Sardiello et al., 2009) are shown in red.

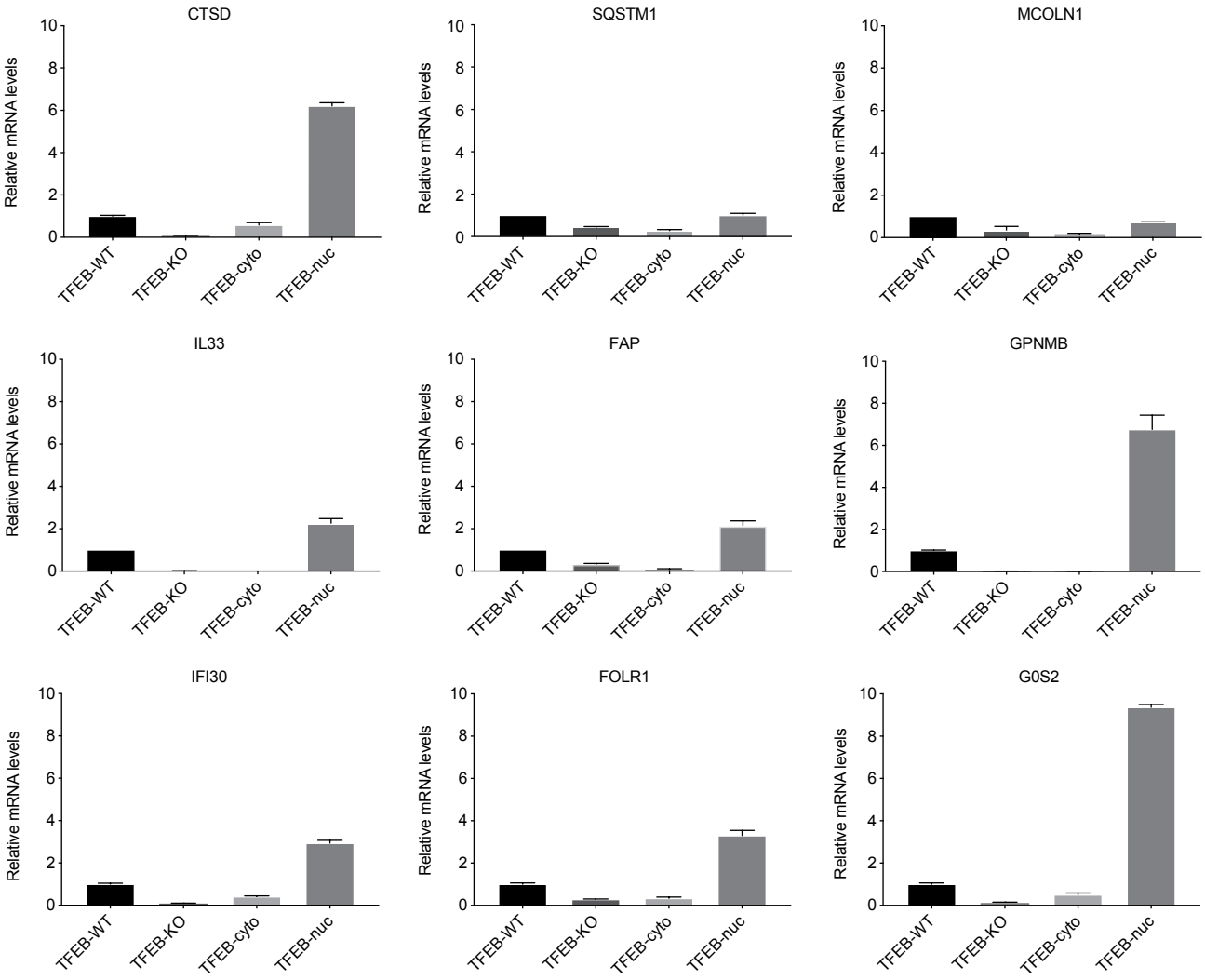

Figure S2. Quantitative PCR analysis confirms TFEB target genes are upregulated in response to TFEB nuclear localization. Related to Figure 2 and Table S2. Gene expression of select TFEB target genes in TFEB-KO, TFEB-WT, TFEB-cyto, and TFEB-nuc cells as quantified by qRT-PCR. Data shown are the average of duplicate wells and representative of three independent experiments. Data are represented as mean +/- SEM (standard error of the mean).

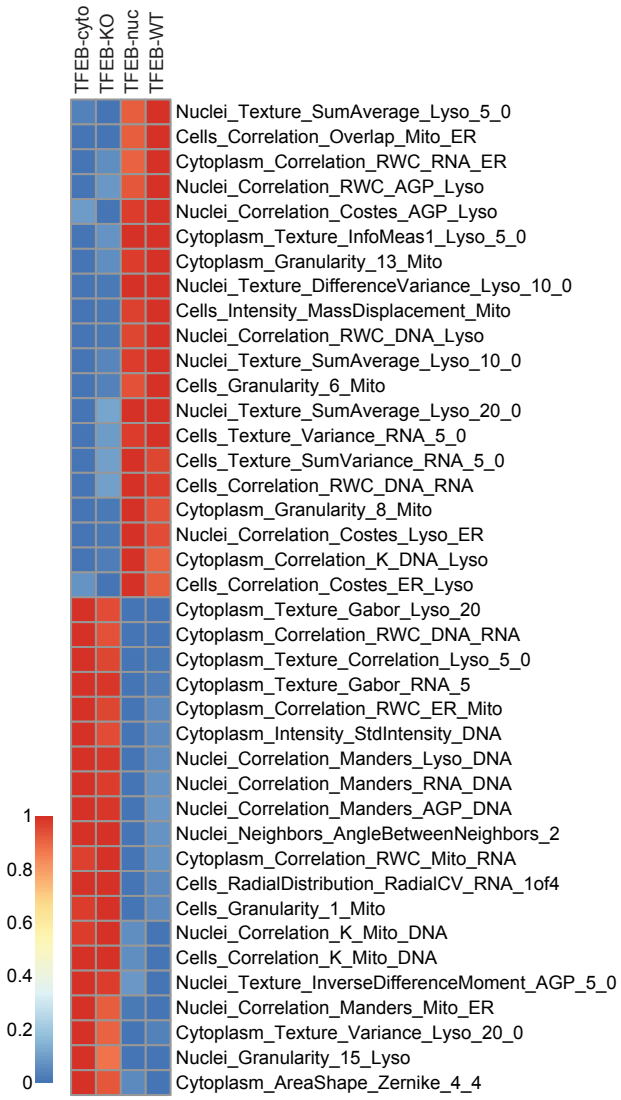

Figure S3. Cell Painting analysis identifies subcellular phenotypic responses to TFEB expression and localization. Related to Figure 3. Heat map representing Morpheus analysis of the most significant cellular features by t-test illustrates phenotypic differentiation of TFEB-WT/TFEB-nuc from TFEB-KO/TFEB-cyto cells. Columns indicate cell type and rows indicate Cell Painting features [Compartment]_[FeatureGroup]_[Feature]_[Channel]_[Parameters] (Bray et al., 2016).

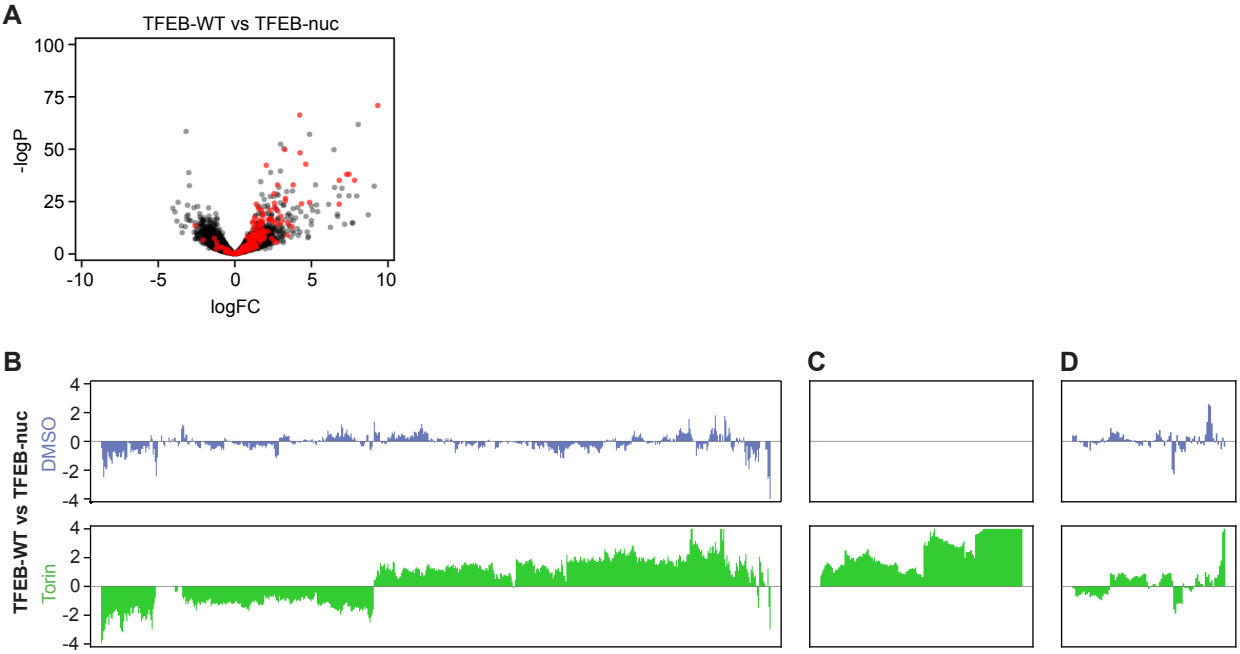

Figure S4. Expression of TFEB-WT, but not TFEB-nuc, upregulated transcription in response to Torin treatment. Related to Figure 4 and Table S4. A) Volcano plot of genes differentially expressed in TFEB-WT cells as compared to TFEB-nuc following Torin treatment. Shown in red are a subset of known TFEB target genes (Table S1) (Sardiello et al., 2009). **B-D)** Panels show differential gene expression at steady-state (DMSO, blue) and with Torin treatment (green). Each bar corresponds to a gene, and the y-axis represents log fold change of differential gene expression (truncated logFC+/-ln4). Genes represented in the bar plots are all genes with significant differential expression (logFC>ln4 or logFC<-ln4 and q-value<0.01) in TFEB-WT relative to TFEB-nuc following Torin treatment. Panel **B** represent genes significantly upregulated with Torin treatment, panel **C** represents genes significantly upregulated with Torin treatment and not transcribed at detectable levels without Torin stimulation, and panel **D** represents TFEB-dependent genes for which transcription did not significantly change in response to Torin stimulation.

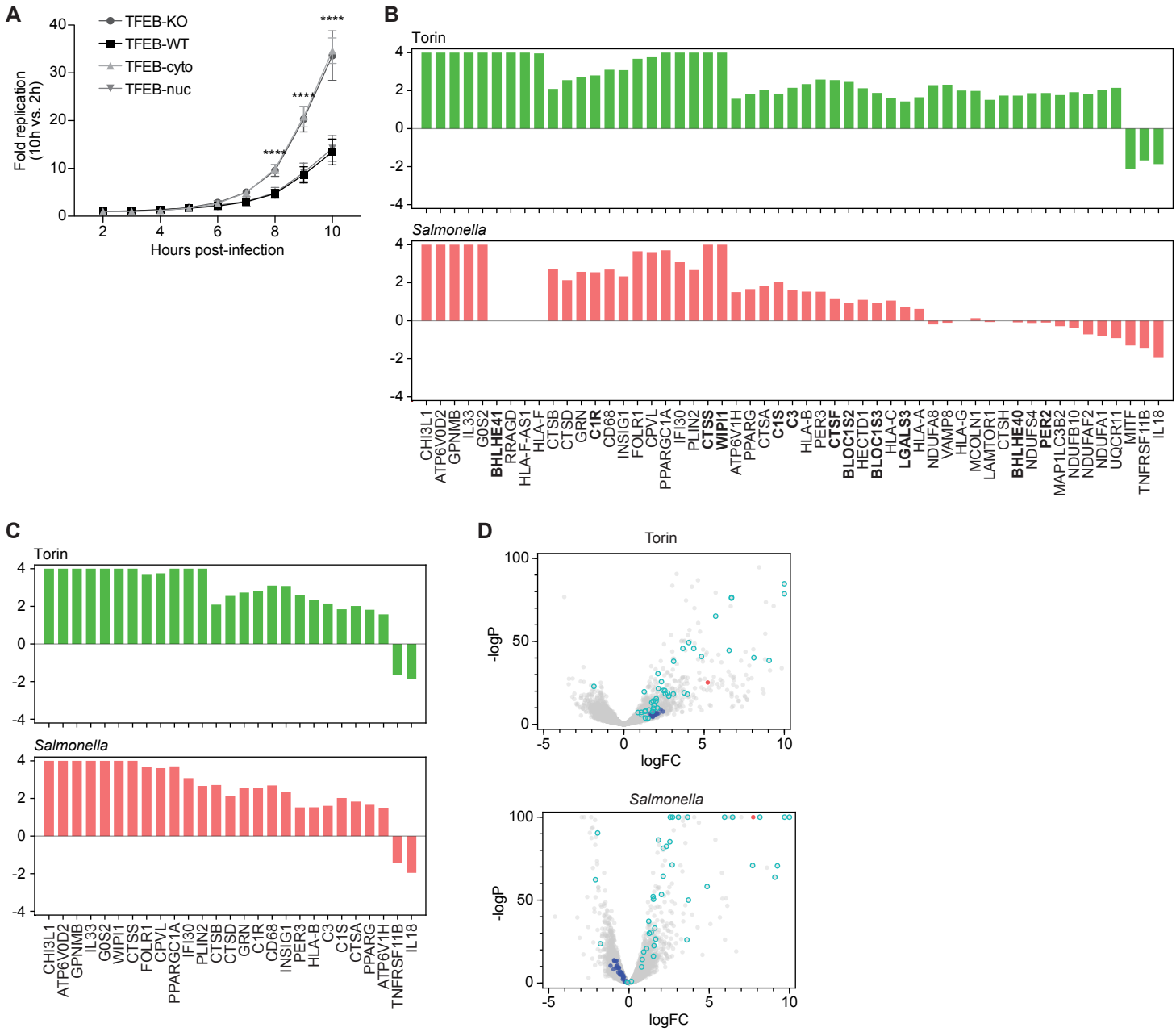

Figure S5. TFEB nuclear translocation is required for transcriptional response and host defense response to intracellular bacteria. Related to Figure 5. A) Intracellular bacterial replication in TFEB-KO, TFEB-WT, TFEB-cyto, and TFEB-nuc cells infected with bioluminescent *S. enterica*. Data shown are the average of eight independent wells and representative of three independent experiments. Data were analyzed using repeated measures two-way ANOVA with Geisser-Greenhouse correction and individual variances computed by Sidak's multiple comparisons test. Data are represented as mean +/- SEM (standard error of the mean). ****p<0.0001. **B)** TFEB-KO and TFEB-WT cells were treated with Torin or infected with *S. enterica* then processed for RNA sequencing analysis. Response of select genes differentially expressed between TFEB-WT and TFEB-KO cells following Torin treatment (logFC>ln4 or logFC<-ln4 and q-value<0.01) are shown. A subset of genes differentially expressed following Torin treatment (green) are also differentially expressed in cells infected with *Salmonella* (pink). **C)** TFEB-KO and TFEB-WT cells were treated with Torin or infected with *S. enterica* then processed for RNA sequencing analysis. Select genes differentially expressed between TFEB-WT and TFEB-KO cells in response to both Torin treatment (green) and *Salmonella* infection (pink) (logFC>ln4 or logFC<-ln4 and q-value<0.01) are shown. **D)** Volcano plots illustrate differential gene expression from TFEB-KO and TFEB-WT cell lines treated with Torin (top) or infected with *S. enterica* (bottom). TFEB (red) and select genes functioning in autophagy, lysosome and immune responses (cyan) and mitochondrial respiration (blue) are highlighted.

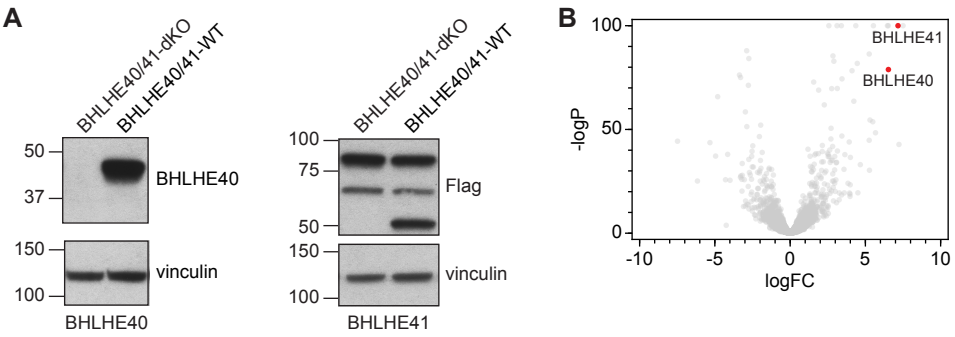

Figure S6. Re-expression of BHLHE40 and BHLHE41 in BHLHE40/41-dKO cells is detected by immunoblot and RNA sequencing. Related to Figure 7. A) Immunoblots demonstrate BHLHE40 and BHLHE41 proteins are detected with anti-BHLHE40 and anti-Flag antibodies, respectively, in BHLHE40/41-WT but not BHLHE40/41-dKO cells. Vinculin serves as a loading control. Data are representative of at least two independent experiments. **B)** BHLHE40/41-dKO and BHLHE40/41-WT cell lines were processed for RNA sequencing analysis. As compared to dKO cells, BHLHE40 and BHLHE41 transcript levels (red) are significantly increased upon reconstitution.